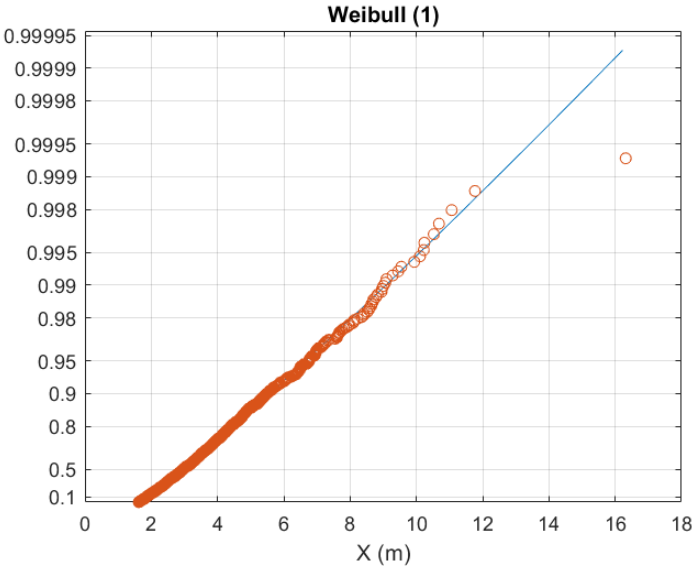


Report

Interrupt Criteria for DP-operated Devices

Author(s)

Karl E. Kaasen
Halgeir Ludvigsen



Address:

NO-
NORWAY

Enterprise /VAT No:

Report

Interrupt Criteria for DP-operated Devices

REPORT NO.	PROJECT NO.	VERSION	DATE
OC2022 F-100	302006948	1	2022-10-05

KEYWORDS:

Marine technology
Hydrodynamics
Marine operation
Interrupt criteria
Statistics
Semi-submersible
Dynamic Positioning
Weibull distribution
SIMO

AUTHOR(S)

Karl E. Kaasen
Halgeir Ludvigsen

CLIENT(S)

The Petroleum Authority of Norway

CLIENT'S REF.

Lars Geir Bjørheim

NUMBER OF PAGES/APPENDICES:

48

CLASSIFICATION

Restricted

CLASSIFICATION THIS PAGE

Restricted

ISBN

ISBN

ABSTRACT

A study has been carried out to find an approach to calculate Hs-Tp criteria for when a marine operation must be interrupted due to forthcoming adverse wave conditions. The work is limited to considering the vessel's surge motion. The basic limit is on surge offset. This limit can be equivalently expressed as a contour line in the Hs-Tp plane. A probabilistic approach is used. Based on simulated time series of response, a probability function of local maxima is fitted to the data. The 3-parameter Weibull distribution was found to represent the total response (wave frequency + low frequency) well. The distribution was used to find extreme offset in a 3-hour interval and quantiles of offset. For two semisubmersible vessels, tables of wave-state dependent probability of limit exceedance is calculated, and limiting Hs-Tp contours are presented. The approach assumes that wave forecast is available. A suggestion is given for how to use alpha factors in the calculation to account for uncertainty in the forecast. Suggestions for further topics of work are given.



PREPARED BY

Karl E. Kaasen

CHECKED BY

Halvor Lie

APPROVED BY

Henning Braaten

Dokumentet har gjennomgått SINTEFs godkjenningsprosedyre og er sikret digitalt

Document History

VERSION	DATE	VERSION DESCRIPTION
0	2022-09-18	Draft
1	2022-10-05	Final Version

Table of Contents

1	INTRODUCTION	5
1.1	Objective	5
1.2	Marine operations	5
1.3	Response limits	5
1.4	Alpha factor.....	5
2	MODELS	6
3	RESPONSE STATISTICS.....	8
3.1	Base case.....	8
3.2	Statistical analysis of base case.....	8
3.3	Effect of swell.....	15
3.4	Effect of wind	16
3.5	Effect of pitch on local surge.....	17
4	ESTIMATION OF EXTREME RESPONSE.....	20
4.1	Theoretical approach	20
4.2	Data-driven approach	21
4.3	Smoothness of process	21
4.4	Fitting probability model.....	22
4.5	Extreme value estimation	27
4.6	Estimation error	29
4.7	Application in probabilistic decision making	30
4.7.1	Probability calculation	30
4.7.2	Effect of alpha factor	31
4.7.3	Simplified, conservative calculation	31
5	RESULTS	33
5.1	Parameters.....	33
5.2	Results for Deepsea Bergen	33
5.3	Results for the Exwave semi	39
6	SUGGESTIONS FOR FURTHER WORK.....	45
6.1	Error analysis.....	45
6.2	Choice of threshold	45
6.3	Theory-based approach and combining LF and WF extremes.....	45
6.4	Effect of rate limits.....	45
6.5	Multi-mode and composite response criteria	45
7	CONCLUSION.....	46

8	ACKNOWLEDGEMENT.....	47
9	REFERENCES.....	47

1 INTRODUCTION

1.1 Objective

The objective of the study is to develop a method to calculate criteria for when a marine operation involving a DP-operated vessel must be interrupted because continuing the operation would involve a too large risk of exceeding pre-set limits for the vessel motion.

1.2 Marine operations

The marine operations to be considered in this study are assumed to be weather restricted, i.e., their execution depends on fulfilment of given environmental criteria expressed in terms of significant wave height and spectral peak period. It is clearly more difficult to satisfy the criteria for an operation of long duration than a short operation. Let the *operation reference period*, T_R , be defined as:

- a. the time it takes to interrupt an operation and revert or suspend it in such a way that the objects involved in the operation are brought to a safe condition, cf. [9], [10], or
- b. the time it takes to carry out a planned marine operation.

In case (a) the operation may be resumed when permissible according to the criteria. It is assumed that weather forecasts are available during T_R .

T_R is usually composed of two parts, the planned operation period, T_{POP} , and the estimated maximum contingency time, T_C , such that $T_R = T_{POP} + T_C$, cf. [9].

1.3 Response limits

The limiting factors for the execution of the operation are typically the response variables of the vessel or variables derived from these, such as the acceleration at the top of a crane. For a drilling operation the limit could be a certain horizontal offset of the vessel's centre. In the case when the vessel is connected to another by a gangway, several limits will exist for the gangway motion, typically limits for the gangway's longitudinal elongation and contraction, the angular motion of the vessel and the accelerations at the points of support [12], [13].

The criterion for safe operation is that all the relevant response variables are below their respective limits. Assuming that the responses are uniquely determined by the weather state, the limits can be transformed to an equivalent set of limiting weather parameters, such as limiting pairs of significant wave height and spectral peak period. Whether the criterion for safe operation involves single or multiple limits is of no consequence since there will always be a H_s - T_p set that reflects the effective limit.

1.4 Alpha factor

Weather forecast is available from Meteorological institutions with an update rate of up to 1/hour. The accuracy of the forecast decreases with the lead time (the time from when the forecast is made to the time it applies for) The alpha factor reflects the uncertainty. Usually, the operational limit is given as a value of significant wave height, H_s . Assume a limit of $H_s = 5$ m is given for an operation, and an alpha factor of $\alpha = 0.8$ is specified for a certain distance in the future. The H_s limit for the operation at this time ahead then becomes $0.8 \cdot 5.0$ m = 4.0 m, cf. [9].

2 MODELS

Two semi-submersibles of different size and hull geometry are used in the study: the Deepsea Bergen and the Exwave semi. These are the same vessels as was treated in the foregoing project [8]. The hulls are shown in Figure 2-1, and the vessels' main particulars are shown in Table 2-1. The two semis have been extensively tested and analysed in the Exwave JIP [3]. The numerical models for the semis were developed in the Exwave JIP.

For the time domain simulations described in the following, the versatile and efficient simulation program SIMO [5] was used. SIMO contains most of the models needed for studying marine operations, e.g., hydro-mechanics, metocean environment, mooring system and DP-system. For the presents study, SIMO complies fully with the requirements in [10].

An important result from the Exwave JIP is that for a semisubmersible the wave drift load will increase due to viscous loading on the columns, as compared to the loads commonly predicted by potential theory. The increase depends on the wave height and the speed of current. In addition to the viscous force there will be an inviscid effect caused by current. These effects are modelled by the semi-empirical "Exwave formula"[3], [8].

The dependence of the LF wave load on current speed also gives rise to low frequency *damping* (since LF speed is equivalent to current speed in the opposite direction with respect to force). The additional load and damping according to the Exwave formula are included in the SIMO model used in the present study.

For the study, the two semis were equipped with DP system (The real Deepsea Bergen had no DP system at all). Table 2-2 shows the main parameters of the DP system. The position gain (stiffness) was chosen identical (=200 kN/m) for the two vessels. The velocity gains (damping) were chosen such that both vessels will have a damping ration of 70% in addition to the natural, hydrodynamic damping.

In Table 2-2 "sufficient" capacity means that the thrusters will cope with any realistic thrust demand from the controller without saturating. Basically, the response models are linear, yet the limit of 14 seconds on the thrusters' rise time may introduce nonlinearity when there is a demand for quick change in the thruster force.

Further description of the numerical models is given in [8].

Table 2-1 Main particulars of the two semis

		Deepsea Bergen	Exwave semi
Length of pontoons		92.5 m	107.5 m
Width		67.2 m	81.3 m
Draught (survival)		17.5 m	23.0 m
Displacement (survival)		25 963 t	39 206 t
Radii of gyration:	roll	29.4 m	36.1 m
	pitch	31.3 m	34.4 m
	yaw	35.0 m	42.3 m
Width of columns		9 m and 7.4 m (circular)	12.5 m (square)

Table 2-2 DP data

Parameter	Deepsea Bergen	Exwave semi
Position gain	200 kN/m	200 kN/m
Velocity gain	3 400 kN/(m/s)	4 200 kN/(m/s)
Filter bandwidth	1/30 Hz	1/30 Hz
Filter damping ratio	70 %	70 %
Rise time of thrusters	14 s	14 s
Capacity of thrusters	Sufficient	Sufficient

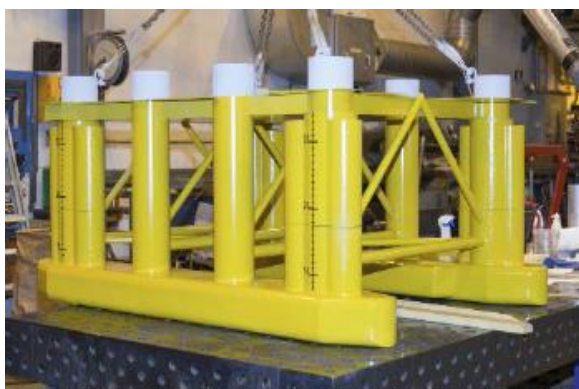


Figure 2-1 Deepsea Bergen (left) and the Exwave semi (Models at SINTEF Ocean's laboratory)

3 RESPONSE STATISTICS

3.1 Base case

The "base case" is one environmental condition and one vessel model that are chosen for study of the response process. The Base case will be used for familiarisation with the response process and development of methods for analysis and processing. The model for the Deepsea Bergen is chosen.

The base case environment is shown in Table 3-1. The sea state represents a typical average condition. The current speed of 0.5 m/s is rather high for Norwegian waters. It is a heritage from the previous project [8], where a point a point was made of demonstrating the effect of the so-called Exwave correction to the wave drift load. A constant current speed will not cause any dynamic excitation by itself, but amplify the wave excitation. In addition, the current will increase the damping (which will to some extent counteract the rise in excitation). The environmental condition is simple and clear-cut in the sense that the wave and current are collinear, and no wave directional spreading is modelled. Only the vessel's surge response is considered, as this is sufficient for the purpose of the study.

In some cases, the parameters of the base case are changed to see the effect on the results. In these cases, the base case can be considered as a sort of zero point or reference for the variation.

Table 3-1 Base case environment

Wave	Wave spectrum type:	JONSWAP
	Significant wave height (H_s):	5 m
	Spectral peak period (T_p):	11.8 s
	Gamma parameter (-):	1.0
	Direction of propagation:	0 °
Current	Speed:	0.5 m/s
	Direction:	0 °
Wind	None	

3.2 Statistical analysis of base case

A sample function (time series) of 100 hours duration is simulated with SIMO using Deepsea Bergen model and the environment in Table 3-1. The simulation was done with a time step of 0.5 seconds. Hence, each response variable counted 720 000 points. Figure 3-1 shows the spectrum of surge motion. The LF component is seen to be predominant. Still, dominates, there is an appreciable amount of WF motion (The WF and LF parts have been separated with a sharp filter with sharp cut-off at 1/30 Hz). The standard deviations and sample maxima of the components are shown in Table 3-2. The ratio of maximum to standard deviation is 4.71 for the WF motion and 7.55 for the LF motion. This demonstrates that the two processes are fundamentally different. (It is interesting to note that the large difference in ratio exists even when the number of LF peaks in the sample is only 1/6 of the number of WF peaks)

The statistical distribution of the local maxima of WF motion is known to be close to the Rayleigh distribution (theoretically exact for an infinitely narrow-banded gaussian process [1], [2]). For the simulated 100-hour WF process, and assuming the Rayleigh distribution applies, the theoretical most probable extreme becomes 4.55 times the standard deviation, which is close to the ratio above. Figure 3-4 shows the spectra of wave and WF surge.

The much higher ratio of extreme value to standard deviation for the LF surge component is the consequence of wavedrift load being exponentially distributed. According to Stansberg [7], the LF response will be close to the exponential distribution too when the damping is high, which is the case for a dynamically positioned vessel.

Figure 3-2 and Figure 3-3 show the surge response around the largest total and largest LF response. For the *total motion*, the ratio of maximum to standard deviation is 6.57. This ratio will depend on the relative magnitudes of LF and WF motion.

The distributions of total surge, LF surge and WF surge are shown in Figure 3-5. While the WF component is fairly symmetrical, the LF component is clearly skewed, which also makes the total surge motion skewed. The LF motion is clearly not exponentially distributed across its entire domain (which includes negative values), but could approximately be so above a certain positive value ("exponential tail").

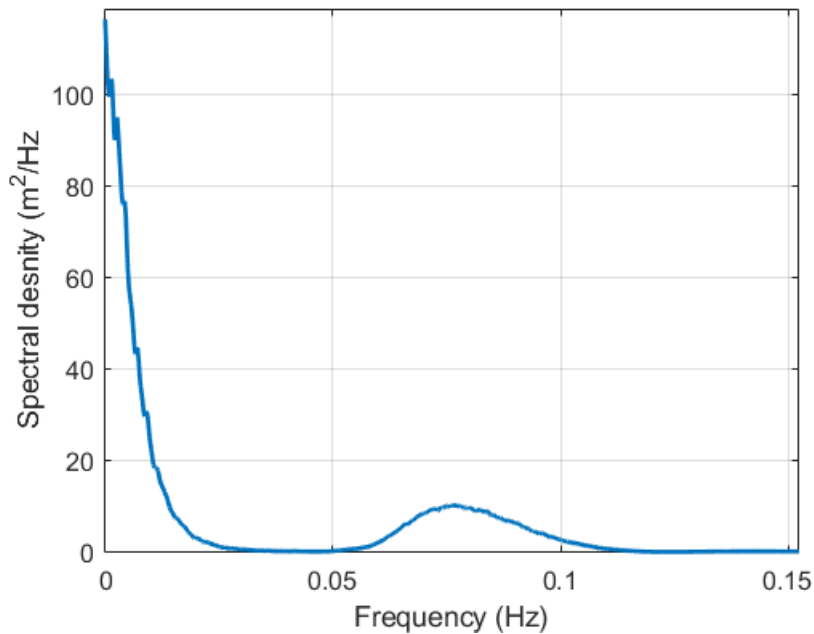


Figure 3-1 Power spectrum of surge motion ($H_s = 5$ m, $T_p = 11.8$ s)

Table 3-2 Standard deviations of 100 hours of simulated surge

Component:	Total (LF+WF)	LF	WF
Standard deviation:	1.036 m	0.877 m	0.552 m
Sample maximum;	6.81 m	6.60 m	2.600 m

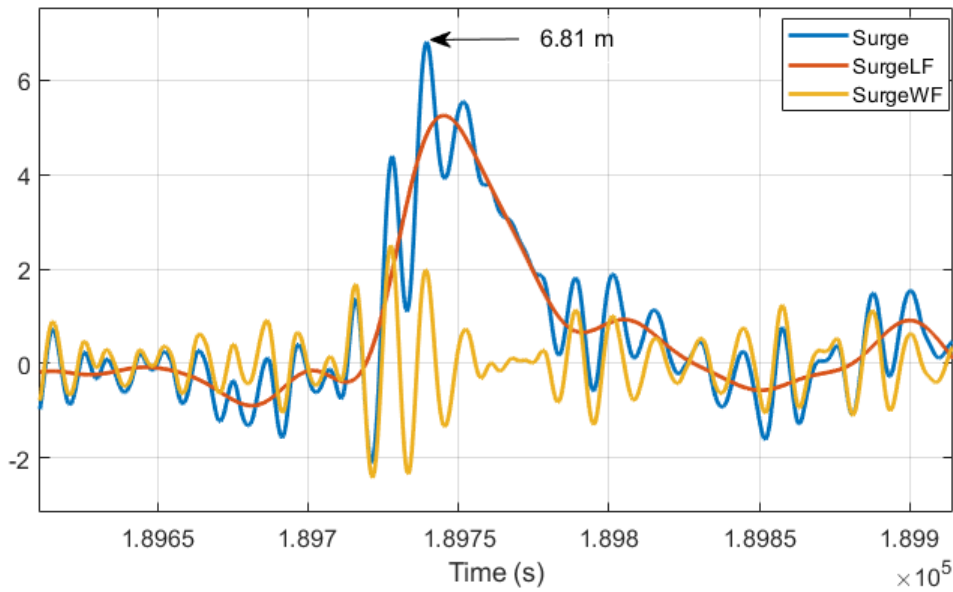


Figure 3-2 Total surge, LF surge and WF surge. Part of 100 hours simulation shown, including sample maximum

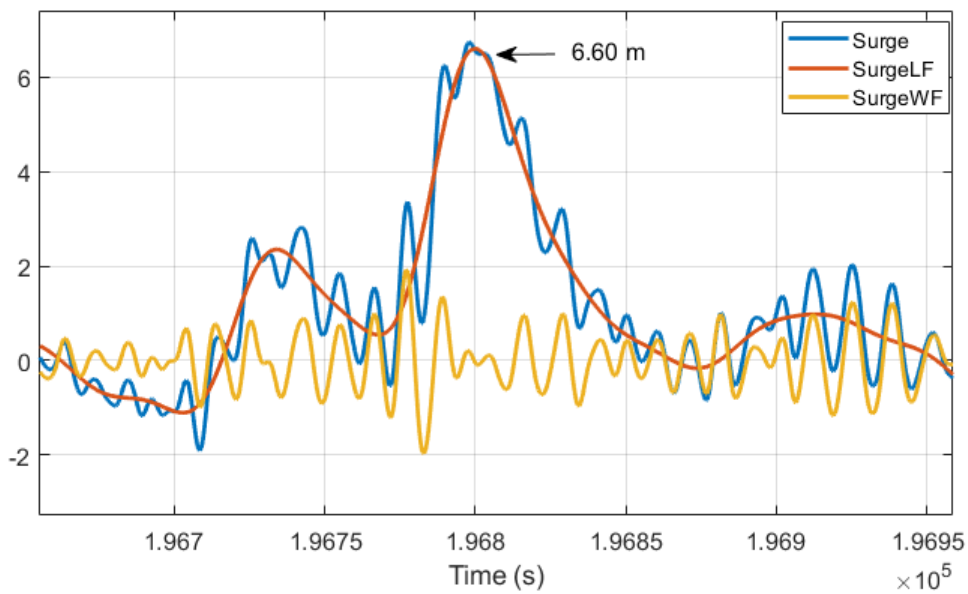


Figure 3-3 Total surge, LF surge and WF surge. Part of 100 hours simulation shown. Largest LF surge indicated.

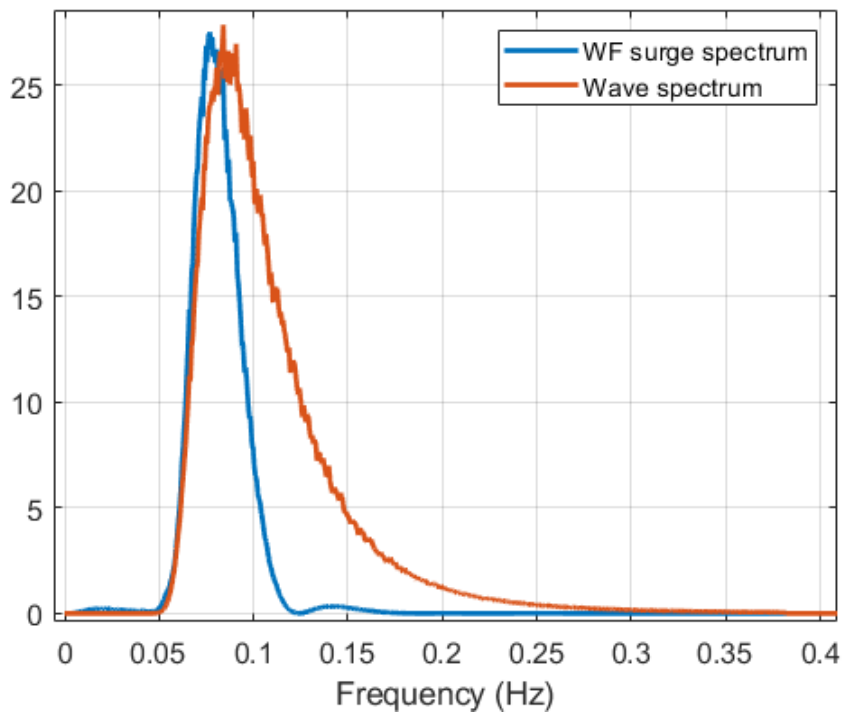


Figure 3-4 Spectra of wave and WF surge (the latter scaled in height for better comparison). $H_s = 5$ m, $T_p = 11.8$ s.

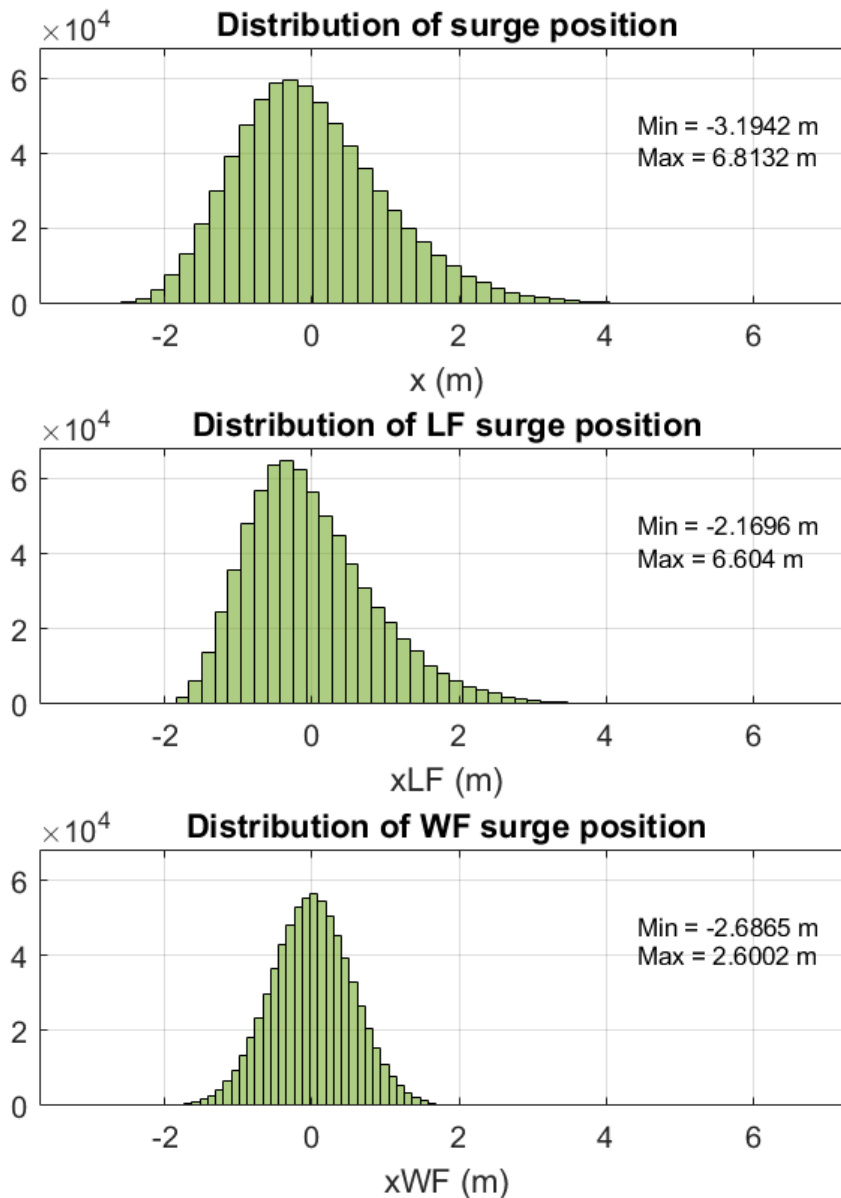


Figure 3-5 Distributions of the 720 000 points of total , LF and WF surge offset

The autocorrelation function of the motion is shown in Figure 3-6 (It is the inverse Fourier transform of the spectrum in Figure 3-1). The high autocorrelation of the WF component is clearly seen, but vanishes after three periods. For the total signal, there is little correlation after 50 seconds and almost none after 100 seconds. For a gaussian process, low correlation implies weak dependence. In statistical estimation, it is often a requirement that the data must be independent. Hence, a false assumption of independence may lead to wrong conclusions in probabilistic and statistical studies, cf. [17]. For a non-gaussian process, the degree of dependence does not automatically follow from the correlation. However, the process of vessel motion does not differ so much from a gaussian process that the correlation is not significantly informative about dependence.

The distribution of upward peaks (local maxima) is shown in Figure 3-7. The distribution resembles that of the continuous signal in Figure 3-5, but is shifted towards the right. Figure 3-8 shows the autocorrelation function of upward peaks. As seen, the correlation is small across five peaks or more (the reason why the function does not approach zero asymptotically is that the mean value of the peaks is non-zero).

Figure 3-9 shows the distribution of LF upward peaks (The number of peaks is 5715, which makes the distribution appear less smooth than that in Figure 3-6). As shown in Figure 3-10, the correlation between neighbouring LF peaks is small (0,2). This is supported by the contours of the joint distribution of neighbouring peaks in Figure 3-11 (had there been significant correlation, the iso-curves would be elongated along the diagonal from the lower left corner to the upper right). The shape of the contour lines indicates that the autocorrelation does not depend significantly on the response (for a gaussian joint distribution, the contours will be ellipses)

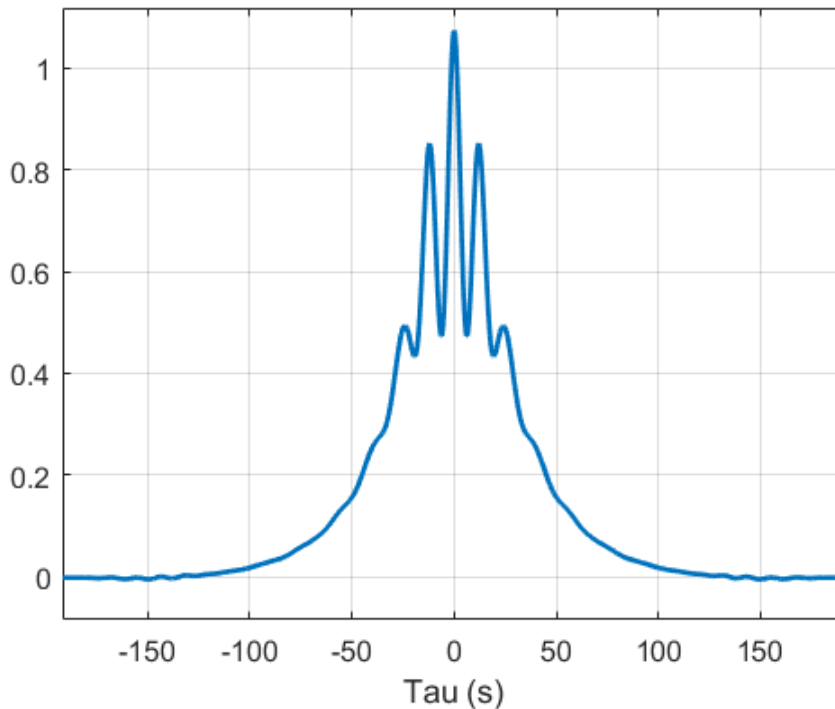


Figure 3-6 Autocorrelation of total surge

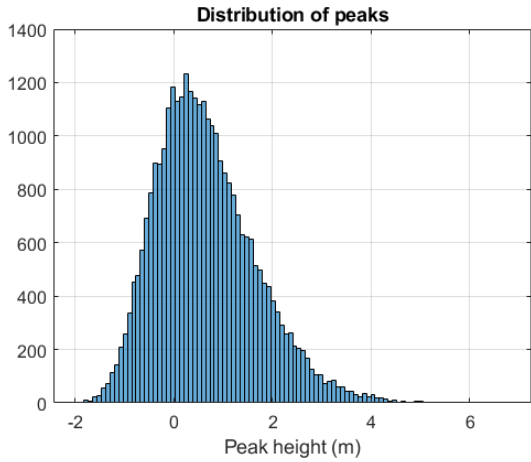


Figure 3-7 Distribution of local maxima (upward peaks). The number of peaks is 31622

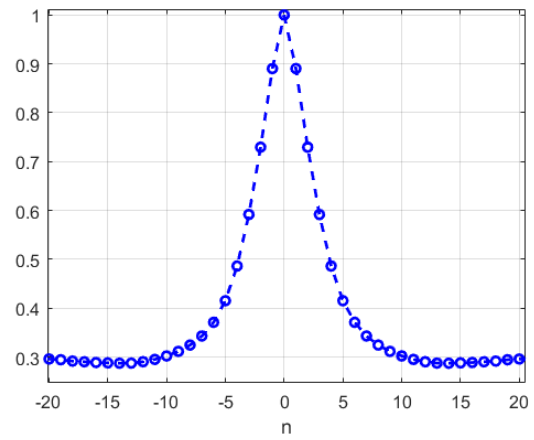


Figure 3-8 Autocorrelation function of local upward peaks. n denotes peak number. The least and largest separation between neighbouring peaks are 1.5 s and 37.5 s, respectively. The mean separation is 11.6 s.

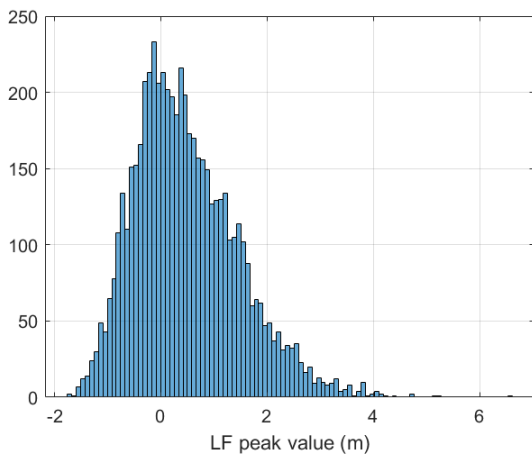


Figure 3-9 Distribution of LF peaks (5715 peaks with a mean separation of 63 seconds)

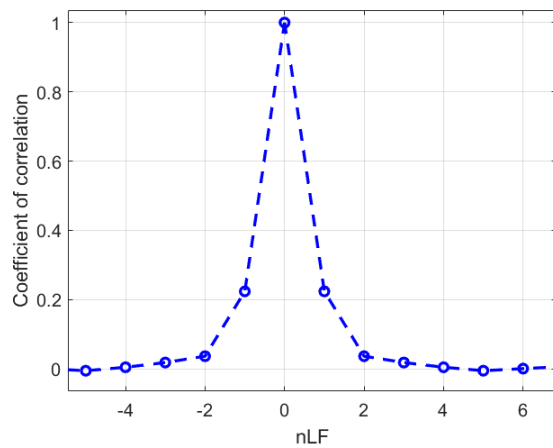


Figure 3-10 Autocorrelation of LF peaks

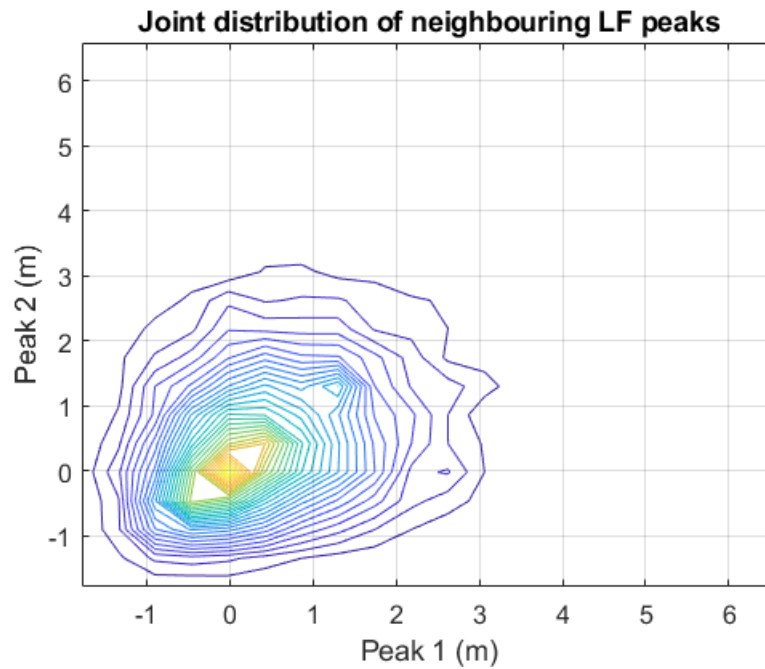


Figure 3-11 Joint distribution of neighbouring LF peaks

3.3 Effect of swell

The results in section 3.2 were made without swell or wind. To investigate the effect of swell, simulations of three hours length were carried out with the base case environment (Table 3-1) and added swell of 1 m and 2 m amplitude and 17 s period. The result is shown in Table 3-3 and as cumulative distribution functions in Figure 3-12 as presented by the SINTEF Ocean workbench SIMA) and indicates that swell has little effect on the extreme surge response. From these cases it appears that swell is of minor importance. Actually, the largest sample maximum occurred for the no-swell case. This is probably due to ordinary statistical uncertainty.

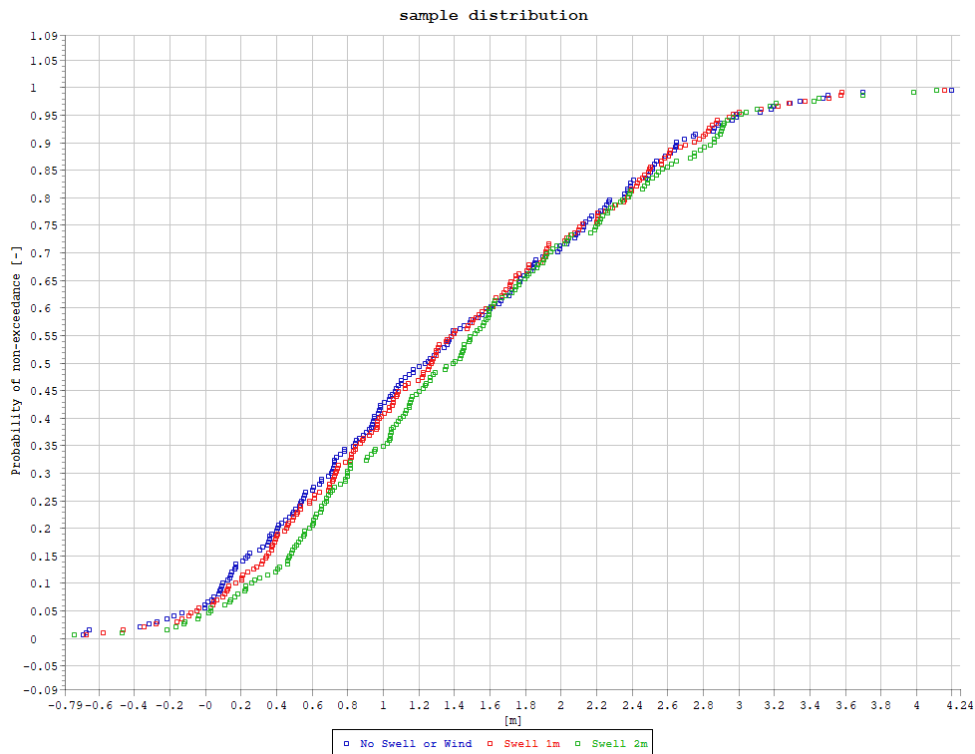


Figure 3-12 Cumulative distribution of maxima in 3 hours. Base case with and without swell. Blue points: No swell, red points: Base case + 1 m swell amplitude, green points: Base case + 2 m swell amplitude

Table 3-3 Simulation maxima corresponding to distributions in Figure 3-12

Case	Max (m)
No swell	4.196
Swell 1 m .	4.154
Swell 2 m	4.110

3.4 Effect of wind

Three cases of wind, collinear with the waves, were simulated for 3 hours duration, see Table 3-4 and Figure 3-13. Wind speeds of 10 m/s, 14 m/s and 18 m/s were tested, the middle speed typical for the base case wave height of 5 m (Table 3-1), cf. [14]. Wind gust was modelled according to ISO-19901-1 [15]

The response appears to depend significantly on wind. The wind load is proportional to the square of the wind speed. Consequently, the speed 14 m/s will give twice as big load as the speed of 10 m/s, and the factor for the highest speed becomes more than three. Still the results are unexpected. Wind load is static with a moderate dynamic variation. The ISO spectrum has large, very slow variations at periods of several minutes. Such slow variations should be effectively handled by the DP-controller's integrator. The strong wind dependence of the response in the table and figure is therefore attributed to using too small integral gain in the controller.

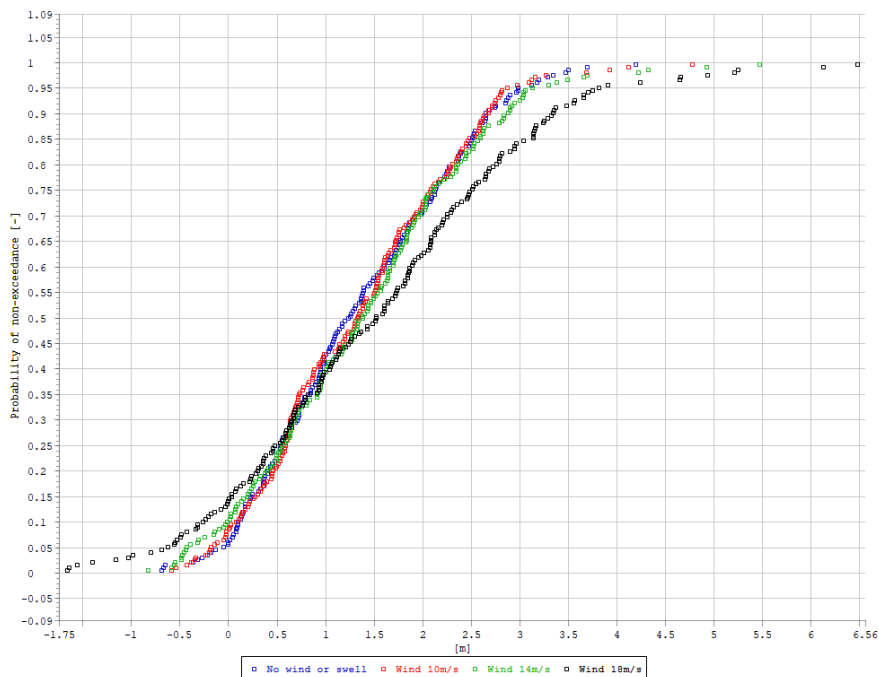


Figure 3-13 Cumulative distribution of surge response without wind and with wind added to the base case waves. Blue points: No wind, Red: wind speed 10 m/s, green: Wind speed 14 m/s, black: Wind speed 18 m/s. Cf. Table 3-4.

Table 3-4 Simulation maxima corresponding to distributions in Figure 3-13

Case	Max (m)
No wind:	4.196
Wind 10 m/s	4.775
Wind 14 m/s	5.468
Wind 18 m/s	6.481

3.5 Effect of pitch on local surge

The surge motion treated so far is the motion at the still water plane. In some cases, the horizontal motion at a certain elevation is of interest. As the vessel's rolling and pitching motion usually take place about axes at the still water level, these components of motion will cause additional horizontal motion at elevated locations in the vessel, e.g. at the support point of a gangway.

The rolling and pitching motions may have distinct resonant periods above the wave periods and below the periods of wave drift motion. For a point above the still water plane, some of this resonant motion will exist in the horizontal motion and possibly cause significant change to its character. To see if such rotation-induced motion is notable for the base case, the surge motion is calculated for a distance c above the still water plane. Neglecting the influence from roll and yaw, the local surge motion at c becomes

$$x_c \approx x + c\theta \quad (1)$$

Here, x is surge at the still water level, c is the height of the considered point, and θ the pitch angle (in radians). The *plus* sign in the expression follows from the axis convention used by SIMO.

For an elevation of $c = 15$ m, the power spectrum of x_c is shown in Figure 3-14. Comparing with the spectrum of x in Figure 3-4, we see that the character of the motion has not changed drastically. While the LF part of the motion is almost unchanged, the magnitude of WF surge at 15 m height is clearly reduced. This is the result of the phasing between surge and pitch. A little "bump" is seen around 0.02 Hz, probably representing the natural period of pitch.

An excerpt of the time series of x_c is shown in Figure 3-15, which is comparable with Figure 3-3. The black line is the pitch-induced surge at 15 m height. It is dominated by WF response and shows no clear resonant motion. From this, we may tentatively conclude that the methods and results presented in Chapter 4 will hold also for surge at other vertical locations in the vessel.

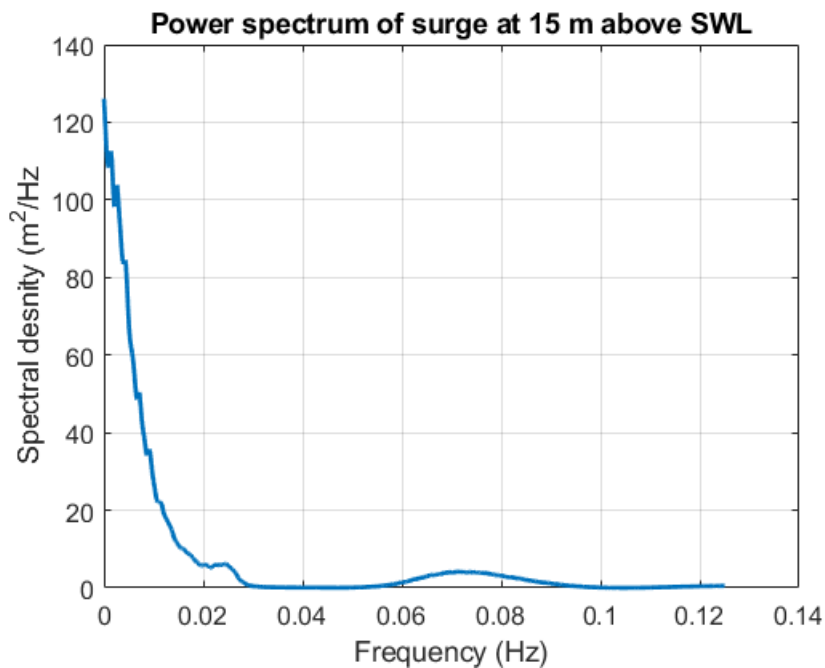


Figure 3-14 Power spectrum of surge motion at $Z_{loc} = 15$ m ($H_s = 5$ m, $T_p = 11.8$ s)

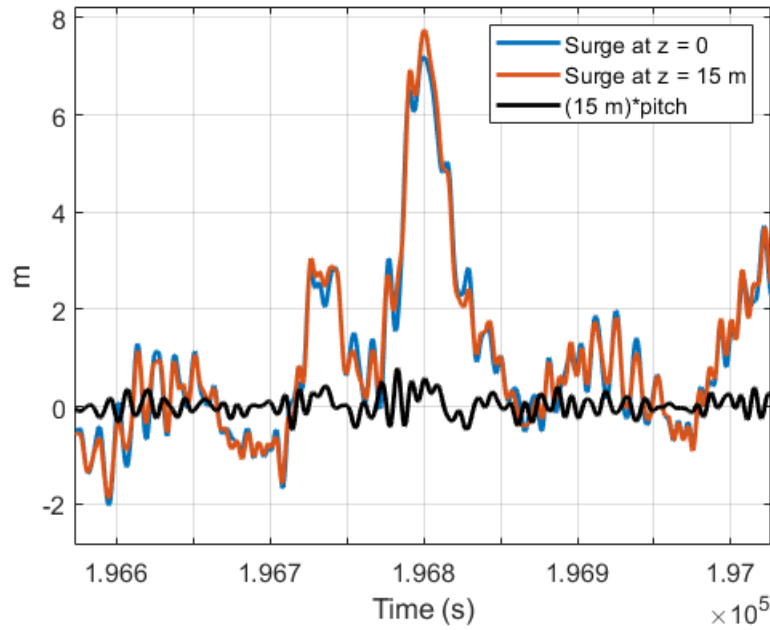


Figure 3-15 Surge motion at SWL and 15 m above SWL ($H_s = 5$ m, $T_p = 11.8$ s)

4 ESTIMATION OF EXTREME RESPONSE

In order to start or continue a marine operation there must be a guarantee that its responses are kept within set limits for the entire duration of the operation. "Guarantee" must be defined as a certain high probability of not exceeding any limit, e.g. 0.99 or 0.9999, depending on the operation and the consequence of failing to keep the operation within the limits. To calculate probability a probability *model* is required. Such a model is typically the cumulative distribution function (CDF) of the variable in question and its derivative, the probability density function (PDF). When these functions are known, one can in principle calculate any quantile, which is the value that has a given probability of non-exceedance. To determine the CDF and PDF, there are two approaches: The theoretical approach and the data-driven approach.

4.1 Theoretical approach

With this approach the probability model is based on theory, i.e. knowledge about the nature of the stochastic process. An important example is estimating extremes of the WF response. Assuming that the peaks of the WF process are Rayleigh distributed the model can be determined by a single parameter: the standard deviation, σ , of the underlying continuous process. The parameter σ can be calculated using simple frequency domain methods, or it can be robustly determined from comparatively short sequences of measurement or simulation.

The LF wave-drift process is more complicated. Still, methods exist for the calculation of its CDF and PDF. The method by Stansberg, described in ref. [7], uses the power spectra of the wave drift excitation and the response. The spectra can be calculated with frequency domain methods, which is done by Mimosa [6].

To combine the statistics of WF and LF response to find an estimate for the extreme total (WF+LF) response in a given period of time (e.g. 3 hours), is complicated [16], and is usually done by rule-of-thumb methods. One much used rule for combination is [4]:

$$x_{ext}^{tot} = \max \left\{ \begin{array}{l} x_{sign}^{LF} + x_{ext}^{WF} \\ x_{sign}^{WF} + x_{ext}^{LF} \end{array} \right\} \quad (2)$$

Here, x is the response variable. "ext" denotes extreme value, and "sign" denotes significant value, defined as two times the standard deviation of x . "Extreme value" can be defined in various ways, e.g. "most probable largest", "expected largest," or a quantile, but it always applies to a duration of time. "Significant value", on the other hand, pertains to the underlying process and is independent of time (for a stationary process).

As an example, the 100-hour extreme according to (2) is calculated for the base case: Since the LF response is the predominant motion type (Table 3-2), the second candidate in (2) applies. Using to the Stansberg method [7], the expected LF extreme surge offset becomes

$$x_{ext}^{LF} = 5.62 \text{ m} \quad (3)$$

This is significantly less than the sample maximum of 6.60 m in Table 3-2. However, the second largest LF peak in the 100-hour time series is 5.25 m, which demonstrates the large spreading of the extremes of the wave-drift process. Hence, the estimate (5) is plausible.

Adding the significant value of the WF surge motion, according to (2), we get

$$x_{ext}^{tot} = 5.62 \text{ m} + 2 \cdot 0.552 \text{ m} = 6.72 \text{ m} \quad (4)$$

This estimate agrees well with the sample maximum of 6.81 m in Table 3-2. Although one cannot draw a firm conclusion from this example, it is an indication that Eq. (2) is a fairly good formula for the total extreme.

Still, it must be expected that a better way of finding the combined LF+WF extreme can be found by forming the joint distribution of LF peaks and the envelope of WF response, as the first step and deriving the total maxima as the second. This problem is treated in the literature, e.g. by Næss [16]. In the present study, this topic is not considered further, except that a check on the correlation between LF peaks and the envelope of the WF motion was made for the base case. This gave a correlation coefficient of 0.23, which may be significant in an evaluation of the total extreme.

4.2 Data-driven approach

In this case a sequence of response data is available from measurement or simulation. A numerical CDF is determined from the data and a mathematical, parametric, CDF *function* is fitted to the data. One important task is to find the best CDF function. Important "standard" candidates are the Rayleigh distribution, the exponential distribution, the Weibull distribution and the Gumbel distribution. For WF response, the Rayleigh distribution is the obvious choice. For LF response the exponential distribution could be a candidate. Now, the Weibull distribution includes both the exponential and the Rayleigh distribution as special cases, and stands out as the best choice. The Gumbel distribution is mainly used to model the largest element in a sample of identically distributed numbers.

The 3-parameter Weibull CDF is defined as

$$F_{Weibull} = 1 - \exp\left(-\left(\frac{x - \theta}{\lambda}\right)^k\right) \quad (5)$$

where x is the stochastic variable, θ the location parameter, λ the scale parameter and k the shape parameter. The distribution is defined for $x \geq \theta$. For $k=2$ and $\theta = 0$ the Weibull becomes the Rayleigh distribution. For $k=1$ the exponential distribution is obtained.

The Gumbel CDF is defined as

$$F_{Gumbel} = \exp\left(-\exp\left(-\left(\frac{x - \mu}{\beta}\right)\right)\right) \quad (6)$$

where μ denotes the location parameter and β the scale parameter. and k the shape parameter. The distribution is defined for all x , positive and negative.

One advantage of the data driven approach is the hypothetical possibility of formulating one model (CDF) for both the WF and the LF offset. If this can be done successfully, the problem of combining the LF and WF extremes into a total extreme by a formula like (2) is circumvented

In the present study, the data-driven approach is chosen. The data is obtained from simulations with SIMO.

4.3 Smoothness of process

When an extreme values is calculated from a distribution fitted to data it is important that the domain of the distribution function includes the extreme value, i.e., the function must be valid for the extreme value. When the largest element of the dataset the CDF is fitted to, is less than the estimated extreme value the estimation has the character of extrapolation. For this to be successful the model (the CDF) must be correct for all values it generates. This means that the underlying dynamic process must be sufficiently smooth. This will probably

hold for the metocean processes and the process of excitation by environmental loads. For the *response* process it must also hold. If the process is a moored vessel, it will hold as long as no line break occurs.

For a vessel with dynamic positioning the force from the thruster system will have an upper limit, which corresponds to a certain offset. If the vessel is driven past the offset limit, the thruster system will saturate and give no more restoring force if the offset increases further. Beyond the limit point the behaviour of the system will change dramatically. It is important, therefore, that no saturation happens when the vessel is within its operational limits.

4.4 Fitting probability model

The data for the model fitting is the 100 hours of simulated surge motion for the base case, i.e., Deepsea Bergen and the metocean data in Table 3-1, see the analysis in Chapter 3. The data is split into WF and LF motion by applying a sharp separation at 1/30 Hz.

According to [9] the maximum duration of a planned weather-restrictive operation is 72 hours. There is consequently good chance a simulated sample function of 100 hours length will contain one or more rare extremes.

Calculations were done with Matlab, using software written in Matlab code. The Weibull and Gumbel distributions were considered to be the most relevant candidates.

A number of methods for the model fitting were used. In Table 4-1 they are listed by the keywords used in the estimation software. The methods can be used on both the total surge, the LF surge and the WF surge. Hereafter "peak" is taken to mean upward peak, i.e., a local maximum

Table 4-1 Options for fitting of cumulative distribution function to response data

ALLPEAKS	All the peaks are used.
INTERVAL	The largest value in intervals of given length
UPCROSSING	The largest peak between zero up-crossing and zero down-crossing

For all options, a threshold can be set, such that only points above the threshold are considered. ALLPEAKS is then to mean "all peaks above threshold".

The options were tried with total surge, LF surge and WF surge. For the option INTERVAL an interval length of five minutes was found to give good results (However, some logic in the calculation was needed to avoid cases where maxima adjacent to the interval boundaries had sufficient separation in time to be reckoned as independent). To test the methods on data of different compositions of LF and WF motion, three environments were chosen, as shown in Table 4-2. The case in the middle row is the base case. The simulated duration was 100 hours for all cases.

It is interesting to note that for the WF motion the Weibull distribution could be fitted almost perfectly for all three cases, provided a threshold of zero was used, meaning that only positive peaks were considered. Figure 4-1 shows the result. The k parameter of the Weibull distribution (cf. Eq. (6)) was estimated at $k=1.95$, and θ was found to be -0.031 . These parameter values are close to the theoretical values of $k = 2$ and $\theta = 0$. The parameter β of the Weibull distribution was estimated at $\lambda = 0.787$. The corresponding standard deviation of the initial (almost) gaussian WF process is $\sigma_{WF} = \lambda / \sqrt{2} = 0.556$. This matches well the value in Table 4-2, which is 0.552 (when written with three digits).

One explanation for the good agreement with theory in this example is that the response spectrum is very narrow-banded, which is seen from Figure 3-4

Comment: The axes in Figure 4-1 and following Weibull plots are different from the traditional Weibull axes, in that the axes are *log*, rather than the common *log-log*. This is done to avoid the contraction of points in the upper right part of the figure and to show the nature of the distribution better.

Table 4-2 Data for model fitting. Standard deviations and ratio between WF and LF response

Wave state		σ	σ_{LF}	σ_{WF}	σ_{WF}/σ_{LF}
$H_s = 5$ m	$T_p = 7.1$ s	1.62 m	1,61 m	0.18 m	0.11
	$T_p = 11.8$ s	1.04 m	0.88 m	0.55 m	0.63
	$T_p = 16$ s	1.08 m	0.62 m	0.89 m	1.42

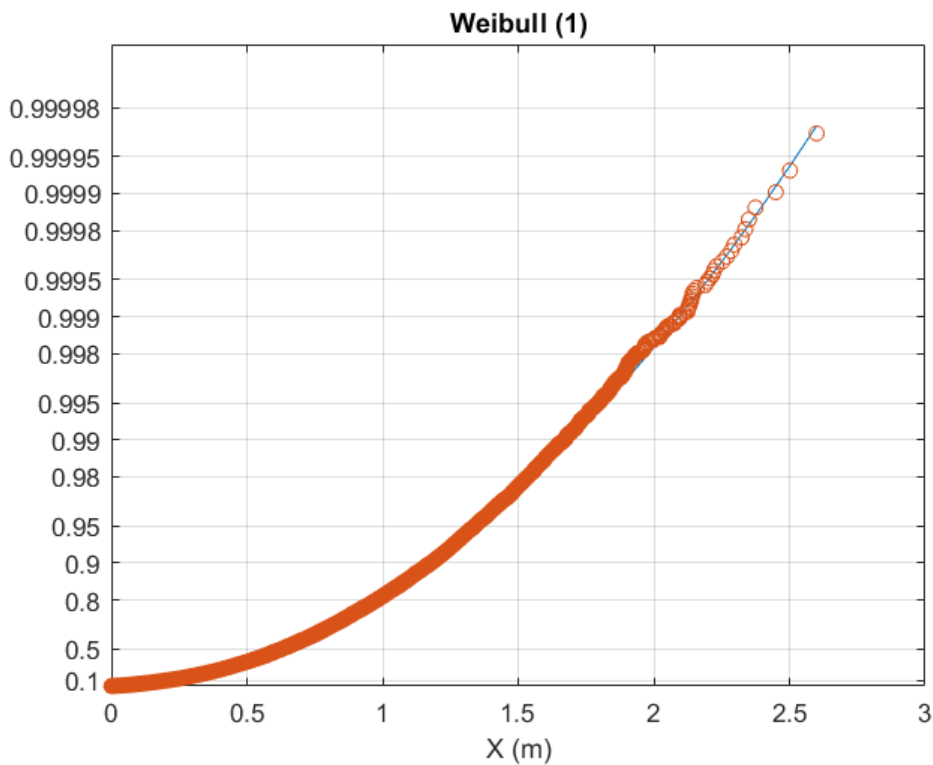


Figure 4-1 Fitting of Weibull CDF to WF surge of base case data ($H_s = 5$ m, $T_p = 11.8$ s). Threshold = 0.

Such excellent results as shown in Figure 4-1 were not obtained for the LF offset or the total offset. However, for the UPCROSSING method with a threshold equal to the standard deviation of the data, quite good results were obtained for the three cases in Table 4-2, see Table 4-3, Figure 4-2, Figure 4-3 and Figure 4-4. It is unexpected that the case with $T_p = 7.1$ s, which has the lowest content of ratio of WF motion, has a larger shape factor k . than the middle case (considering a value of k towards 2 with increasing WF motion).

The case with $T_p=16$ s (Figure 4-4) shows a turn upwards at about $X = 4.5$ m. Why this happens is not known. The effect of this phenomenon is that the fitted probability model will be conservative in extreme value estimation.

The value of the threshold is important. Figure 4-5 shows an example of a poor result, resulting from a threshold value of zero. In this case the estimation method has struggled to fit the model to low peak values that are of no importance for extreme value estimation.

Figure 4-6 shows the Gumbel distribution fitted to the same data as in Figure 4-5 using the INTERVAL method and an interval length of five minutes. The match is just as good as that obtained with Weibull in Figure 4-2. However, on the whole, the Weibull CDF and the UPCROSSING method was found to perform somewhat better than Gumbel and INTERVAL.

As pointed out above, the aspiration is to be able to express the distribution of total surge offset as one CDF and avoid the problem of combining LF and WF statistics. The results above are taken as good enough for this purpose.

Some experimenting with different threshold values was carried out, indicating that thresholds of two or three standard deviations could be better choices. However, more calculations are needed to conclude on this, see suggestions for further work in Chapter 6.

With the UPCROSSING method the average time distance between the peaks is 68 seconds. According to Figure 3-6 the correlation is insignificant for this time separation. This is supported by the actual correlation between the peaks used, which is calculated as 0.089.

Table 4-3 Weibull parameters for total surge offset

Wave state		k	λ (m)	θ (m)
$H_s = 5$ m	$T_p = 7.1$ s	1.0921	1.8422	1.6229
	$T_p = 11.8$ s	1.0463	0.74973	1.0361
	$T_p = 16$ s	1.2100	0.86821	1.0825

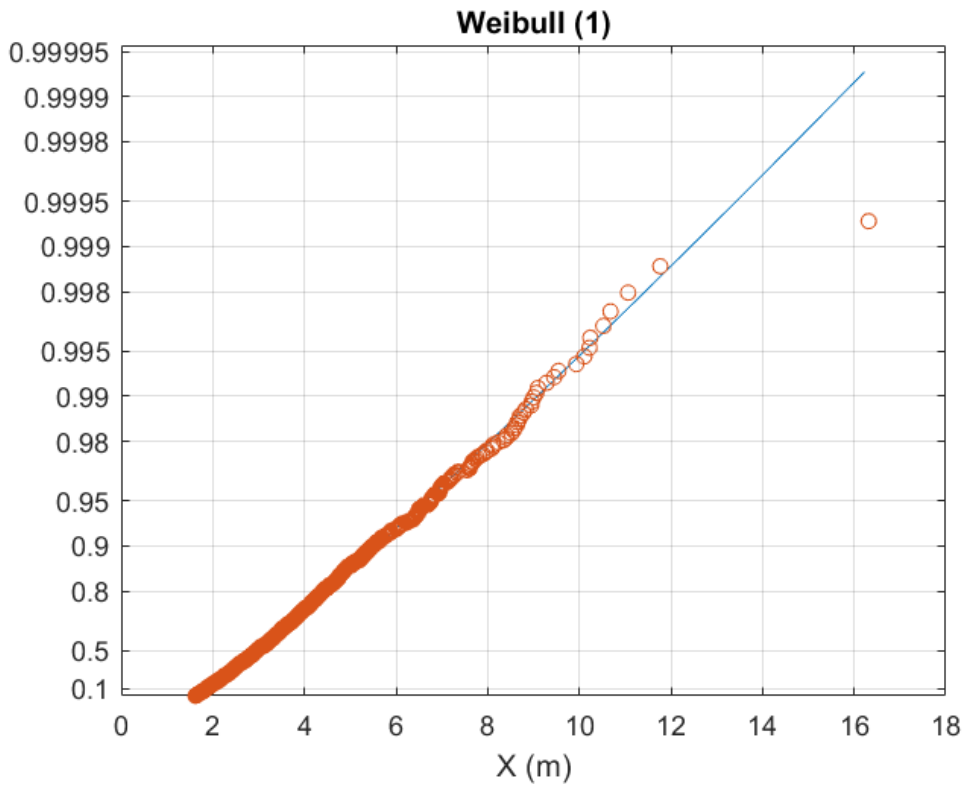


Figure 4-2 $H_s = 5$ m, $T_p = 7.1$ s. Weibull distribution fitted to up-crossing peaks of total offset. Threshold = standard deviation

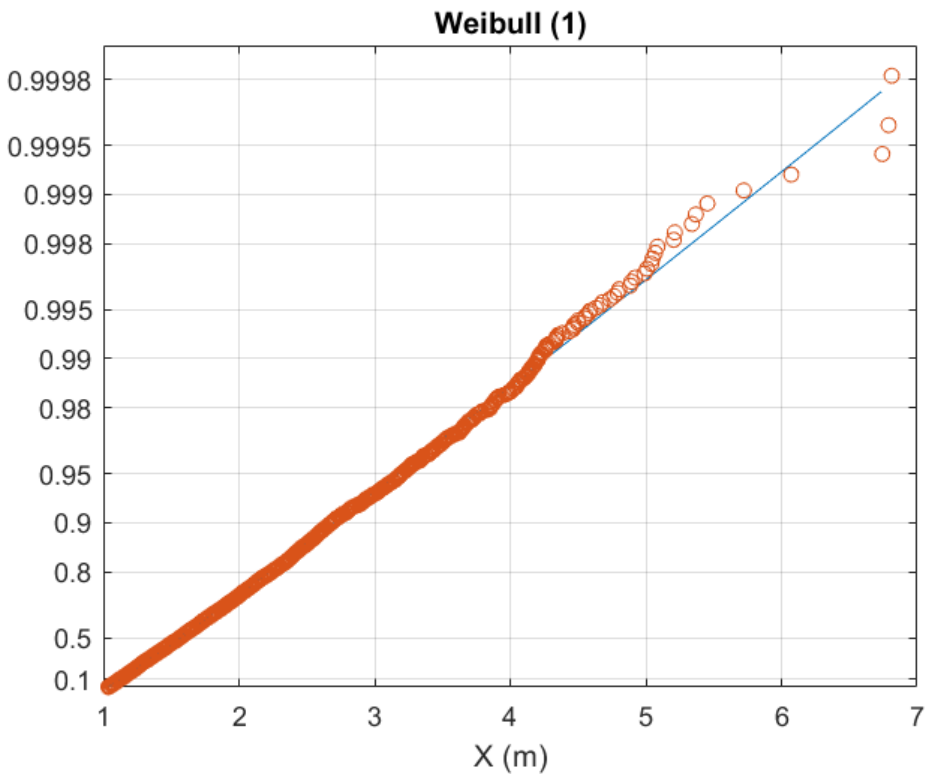


Figure 4-3 $H_s = 5$ m, $T_p = 11.8$ s. Weibull distribution fitted to up-crossing peaks of total offset. Threshold = standard deviation.

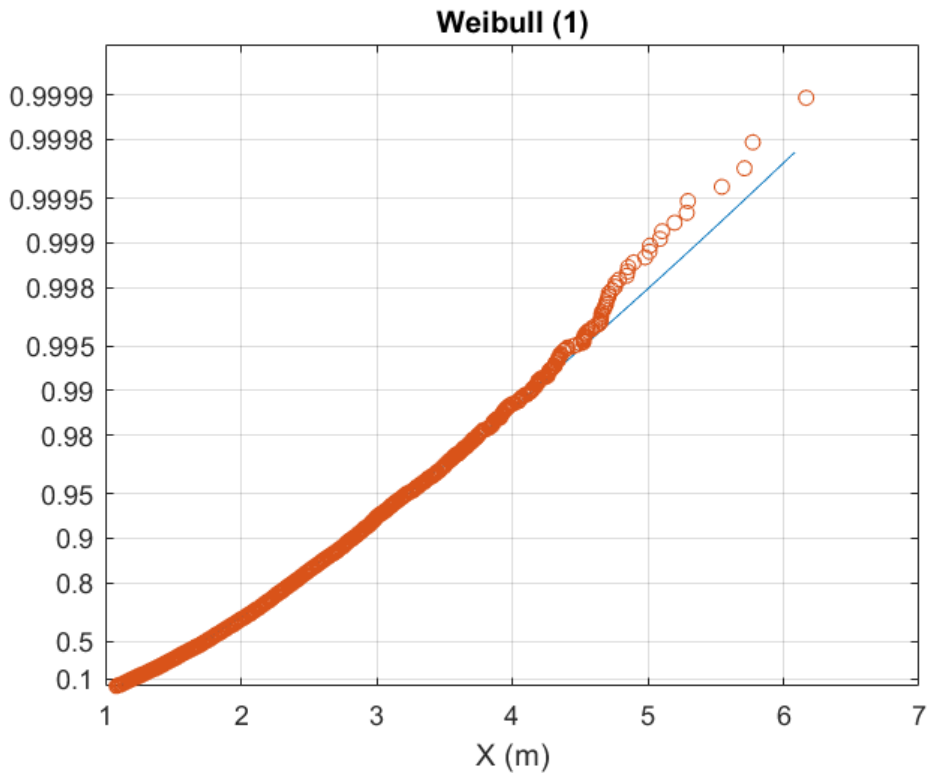


Figure 4-4 $H_s = 5$ m, $T_p = 16$ s. Weibull distribution fitted to up-crossing peaks of total offset. Threshold = standard deviation

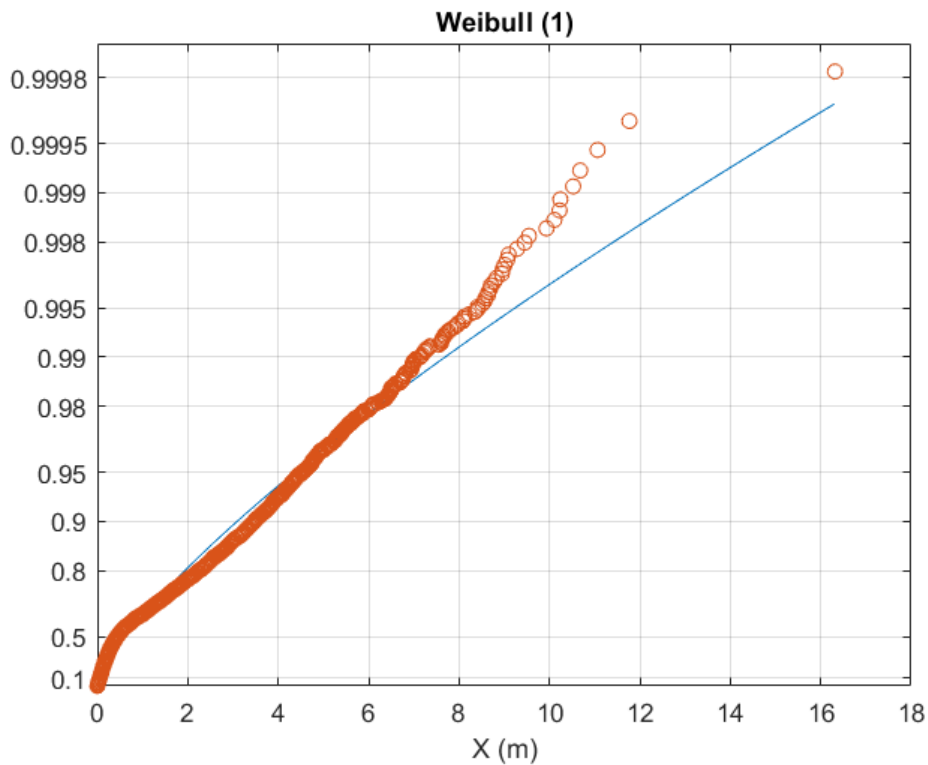


Figure 4-5 The Weibull CDF fitted to data ($H_s = 5$ m, $T_p = 7.1$ s) with the UPCROSSING method and threshold 0. Cf. Figure 4-2.

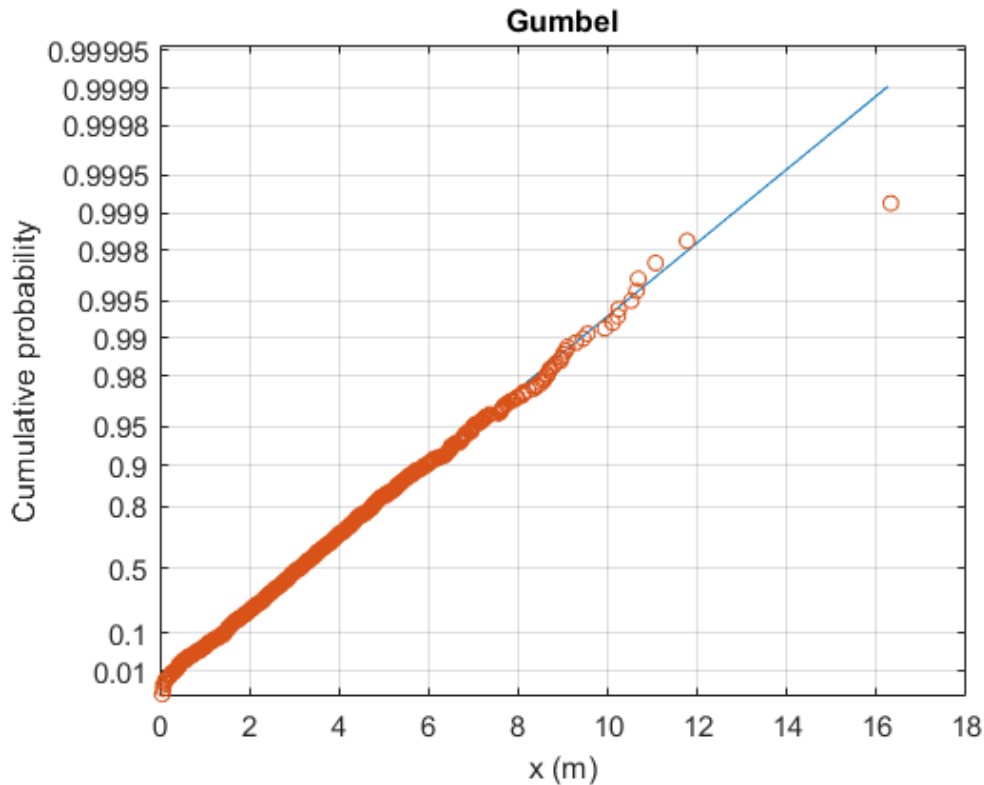


Figure 4-6 The Gumbel CDF fitted to data ($H_s = 5$ m, $T_p = 7.1$ s) with the INTERVAL method (300 s interval length) and threshold 0. Cf. Figure 4-2 and Figure 4-5.

4.5 Extreme value estimation

An extreme value will be defined as a given quantile in a time interval of three hours. The basis for the estimation is the Weibull distribution with parameters that are sea-state dependent as described in the previous section.

Let F be the Weibull CDF found from the data and T_m the mean time between the peaks. For a duration of T (e.g. 3 hours = 10800 seconds), the mean number of peaks is $N = T/T_m$. Provided the peaks are identically distributed and independent, the probability distribution for the largest peak in T is

$$F_L = F^N \quad (7)$$

Let F be expressed in the form

$$F = 1 - \exp(-z(x)) \quad (8)$$

where x is the stochastic variable, and z a function of x . For the Weibull distribution $z(x)$ is

$$z(x) = \left(\frac{x - \theta}{\lambda} \right)^k \quad (9)$$

Inserting (8) in (7) gives

$$F_L = (1 - \exp(-z))^N \quad (10)$$

Rewrite

$$F_L = (1 - \exp(-z))^N = (1 - \exp(-z))^{\exp(z)\exp(-z)N} \quad (11)$$

When z increases toward large values, we have

$$(1 - \exp(-z))^{\exp(z)} \rightarrow e^{-1} \quad (12)$$

which inserted in (11) gives

$$F_L = \exp(-\exp(-(z - \ln N))) \quad (13)$$

We see that z becomes Gumbel distributed, cf. (6). For the Weibull distribution fitted to the bases case.

Figure 4-7 shows F and F_L and their respective density functions when N is 159, which is the number of peaks in 3 hours

For a given probability, $F_L = Q$, the corresponding quantile value, z_Q , for z is solved from (13):

$$z_Q = \ln N - \ln(-\ln Q) \quad (14)$$

The corresponding quantile for x is obtained from (9):

$$x_Q = \theta + \lambda z_Q^{1/k} \quad (15)$$

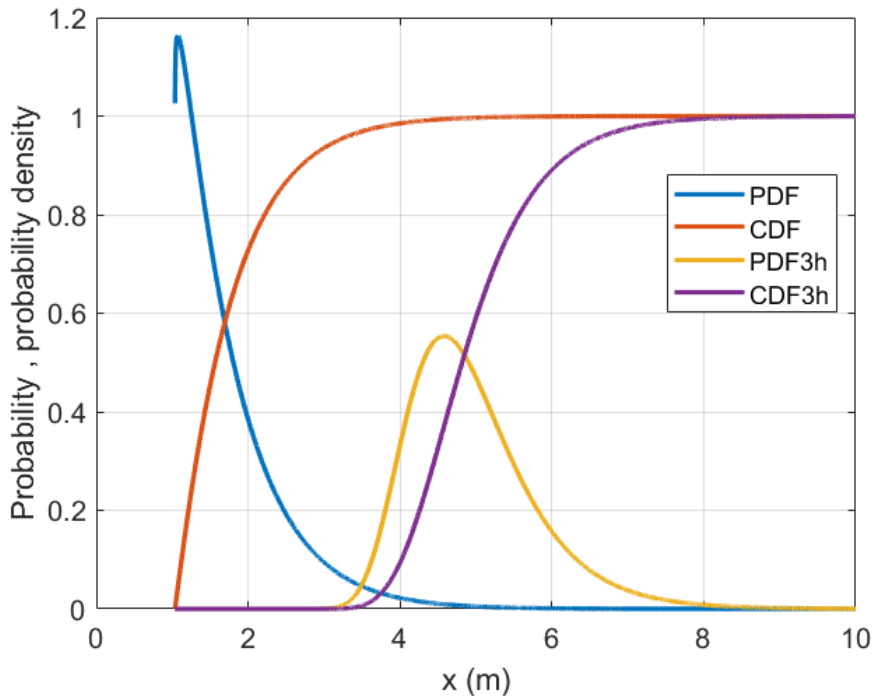


Figure 4-7 Initial Weibull peak distribution (PDF, CDF) fitted to the data, and derived distribution for the largest peak in 3 hours (PDF3h, CDF3h). CDF represents F in Eq. (8), and CDF3h represents F_L in Eq. (10).

4.6 Estimation error

With the data-driven approach the estimated parameters of the distribution are functions of the random data. Consequently, the parameters too will be random, and so will the values of probability calculated with the fitted distribution. Assuming independent data used in the parameter estimation, it is in principle possible to assess the error in the distribution function and correct it in such a way that it accounts for the inherent error.

Estimating error and incorporating its effect in the probability model has not been attempted in the study. However, a test to indicate the importance of the length of the data series was carried out:

The 100-hour simulation of the bases case was split into eight intervals of 12.5 hours length. Weibull distributions were then fitted to each interval, and subsequently used to calculate 3-hour extrema. The results are shown in Figure 4-8. They vary from 4.0645 m to 4.999 m, with a mean value of 4.485 m and a standard deviation of

$$\sigma_{12.5} = 0.281 \text{ m} \quad (16)$$

An estimate for the standard error of the mean value is

$$\sigma_{100} = \sqrt{\frac{\sigma_{12.5}^2}{8}} = 0.099 \text{ m} \quad (17)$$

which also is an estimate for the standard error of the extreme value based on 100 hours of data. Assuming the error to be approximately gaussian distributed around the mean value (4.485 m), a rough estimate for the 3-sigma confidence interval for the extreme becomes

$$[4.188 \text{ m}, 4.782 \text{ m}] \quad (18)$$

Provided the assumption of gaussian estimation error holds, the estimated extreme value will lie in this interval with a probability of 0.997. The variance of the error is inversely proportional to the number of data points. To reduce the interval above by a factor of two, four times as much data is needed, i.e. a time series of length 400 hours.

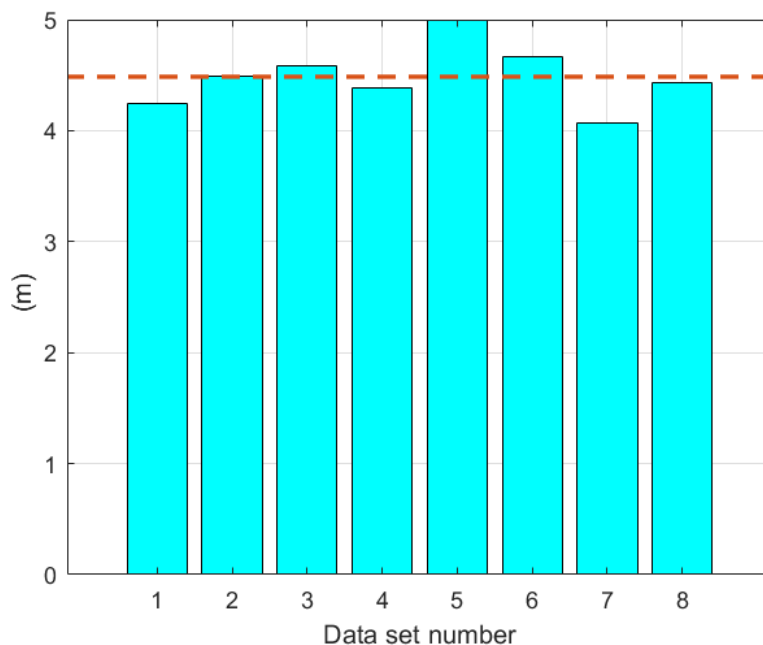


Figure 4-8 Eight estimates of 3-hour extreme value based on data intervals of 12.5 hours length. The dashed line indicates the mean value.

4.7 Application in probabilistic decision making

4.7.1 Probability calculation

It is assumed that some weather-sensitive operation is being executed. Let the T_R be the reference time (cf. section 1.2) for halting the operation, and assume forecasts of H_s and T_p exist for every 3-hour period during T_R . Assume for simplicity that T_R is n 3-hour intervals long, where n is an integer.

Let L be the response limit. We will require that the response x stays below L during T_R with probability Q . Let $P(x, H_s, T_p)$ be the CDF for the largest response variable x during a 3-hour interval. As indicated, P depends on the wave state. The probability that x will not exceed L during the time T_R can be expressed as

$$prob(x \leq L) = \prod_{i=1}^n P(L, H_s^i, T_p^i) \quad (19)$$

Here H_s^i and T_p^i denote the wave states in the n intervals, $i = 1, \dots, n$.

We require that

$$prob(x \leq L) \geq Q \quad (20)$$

If this equality does not hold the operation cannot be wound up in time T_R with the demanded level of safety. This means that the calculation (19) must be carried out at least 3 hours before the beginning of T_R . This implies that (20) must hold in the intervals $i = 0, \dots, n-1$, which is reasonable to assume.

Example:

Let the length of T_R be 12 hours, i.e. this is the time it takes to shut down the operation. The four 3-hour forecast sea states (H_s^i, T_p^i) , $i = 1, \dots, 4$ are

$$\{(4 \text{ m}, 7 \text{ s}), (4 \text{ m}, 8 \text{ s}), (5 \text{ m}, 12 \text{ s}), (6 \text{ m}, 14 \text{ s})\}$$

For an excursion limit of $L = 10$ m, we get the non-exceedance probabilities in Table 4-4. The total probability of non-exceedance of the 10 m limit in 12 hours becomes 0.99216. If the demanded non-exceedance probability is 0.99, this means the operation can go on.

Table 4-4 Exceedance probabilities in 3-hour intervals and total 12-hour exceedance probability. Offset limit = 10 m

i :	1	2	3	4	$P =$ $P_1 \cdot P_2 \cdot P_3 \cdot P_4$ $= 0.992$
Sea state:	$H_s = 4 \text{ m}$ $T_p = 7 \text{ s}$	$H_s = 4 \text{ m}$ $T_p = 8 \text{ s}$	$H_s = 5 \text{ m}$ $T_p = 12 \text{ s}$	$H_s = 6 \text{ m}$ $T_p = 14 \text{ s}$	
Probability, P_i :	0.99503	0.99983	0.99986	0.99742	

4.7.2 Effect of alpha factor

The results in Table 4-4 were made with assumption of known, error-free wave states. To correct for uncertainty in the wave forecast, it common to use alpha factors, which is industry practice today. The purpose of alpha factor is to lower the operational limit (given as a limit on H_s) to account for error in the forecast. According to [9], the alpha factors for the wave heights in Table 4-4 lie in the range 0.83-0.84 for operations of less than 12 hours planned duration.

It is suggested that the wave heights to use in the calculation of probability be the forecast H_s divided by the alpha factor. Thus, the calculation of non-exceedance probability is carried out with a higher wave height than the forecast value.

In [9], the alpha factor is given as a function of the forecast wave height, H_s^F , i.e.

$$\alpha = \alpha(H_s^F) \quad (21)$$

The wave height to use in the calculation becomes

$$H_s = H_s^F / \alpha(H_s^F) \quad (22)$$

Letting the wave heights in the table above now represent the forecast wave height, H_s^F , and using (22), we get the corrected wave states:

$$\{(4.8 \text{ m}, 7 \text{ s}), (4.8 \text{ m}, 8 \text{ s}), (6.0 \text{ m}, 12 \text{ s}), (7.1 \text{ m}, 14 \text{ s})\}$$

(The peak periods are not affected by the correction).

Repeating the above calculation of probability with the corrected wave height gives the results in Table 4-5. The total probability of staying below the limit of 10 m during the close-down time is now reduced to 0.758. This means that, if the demanded probability is 0.99, the operation cannot continue.

Table 4-5 Exceedance probabilities in 3-hour intervals and total 12-hour exceedance probability using corrected wave heights. Offset limit = 10 m

i :	1	2	3	4	$P =$ $P_1 \cdot P_2 \cdot P_3 \cdot P_4$ $= 0.758$
Sea state:	$H_s = 4.8 \text{ m}$ $T_p = 7 \text{ s}$	$H_s = 4.8 \text{ m}$ $T_p = 8 \text{ s}$	$H_s = 6.0 \text{ m}$ $T_p = 12 \text{ s}$	$H_s = 7.1 \text{ m}$ $T_p = 14 \text{ s}$	
Probability, P_i :	0.81837	0.97802	0.98667	0.96027	

4.7.3 Simplified, conservative calculation

With the approach described above, the criterion for interrupting or continuing an operation does not become a function of H_s and T_p only, but of the duration also. As a simpler alternative, the criterion could be based on the wave state in *one* three-hour interval, provided it is made stricter. For example, a worst-case criterion could be used: If the demanded non-exceedance probability for the period T_R is P_{T_R} , and T_R consists of n 3-hour intervals, the probability criterion is satisfied if for *every* interval i , $i=1, \dots, n$, the 3-hour non-exceedance probability, satisfies

$$P_{3h}^{(i)} \geq \sqrt[n]{P_{T_R}}, \quad i = 1, \dots, n \quad (23)$$

If, as in the example in the previous subsection, $n = 4$ and $P_{T_R} = 0.99$, the criterion becomes

$$P_{3h}^{(i)} \geq 0.9975 \quad (24)$$

This clearly conservative criterion must hold for every 3-hour interval and is a function of H_s and T_p .

5 RESULTS

5.1 Parameters

For the two semi-submersibles described in chapter 2, probabilities of limit exceedance are computed for a range of significant wave height and spectral peak period and for a selection of response limits and non-exceedance probabilities. The offset limits for surge were chosen as:

5 m, 7 m, 10 m, 14 m, 20 m

The sea states were chosen as combinations of the following sets of H_s and T_p :

$$H_s \in \{3 \text{ m}, 4 \text{ m}, 5 \text{ m}, 6 \text{ m}, 7 \text{ m}\}$$

$$T_p \in \{4 \text{ s}, 5 \text{ s}, 6 \text{ s}, 7 \text{ s}, 8 \text{ s}, 10 \text{ s}, 12 \text{ s}, 14 \text{ s}, 16 \text{ s}\}$$

This gives $5 \times 9 = 45$ pairs of H_s and T_p , however, nine non-physical combinations were excluded, leaving 36 sea states.

5.2 Results for Deepsea Bergen

For each of the 36 sea states, simulation of 100 hours of surge response was carried out for each vessel. Weibull parameters were estimated for each case, and the Weibull CDF was used for estimation of limit non-exceedance, as described in section 4.2. Table 5-1 - Table 5-5 show the probabilities of non-exceedance for the offset limits above. Probabilities greater than 0.99999 are represented by a "1" in the tables.

The acceptable probabilities for limit exceedance will in general depend on the consequences of failure. The consequences may vary from a certain extra cost to remedy the event to catastrophic. In the following, three levels of non-exceedance probability are chosen:

. 0.99, 0.999, 0.9999

For these probabilities, Figure 5-1 - Figure 5-5 show H_s - T_p contours of constant probability of exceedance. The part of the H_s - T_p domain that satisfies the probability requirement is located below and to the right of the contour lines.

Figure 5-6 - Figure 5-8 show the quantiles of extreme surge offset that correspond to the probabilities above.

Table 5-1 Non-exceedance probabilities for 5 m offset limit (Deepsea Bergen)

$H_s \setminus T_p$	4 s	5 s	6 s	7 s	8 s	10 s	12 s	14 s	16 s
3 m	0.72484	0.0269	0.05434	0.97005	0.99445	0.99990	1	0.99999	0.99996
4 m	-	4.2e-07	2.3e-06	0.29106	0.75398	0.91788	0.98841	0.99503	0.97607
5 m	-	-	3.1e-11	0.00123	0.06809	0.22843	0.62156	0.6283	0.55537
6 m	-	-	-	3.0e-07	0.00014	0.00133	0.04108	0.04722	0.02392
7 m	-	-	-	4.5e-11	3.0e-08	3.4e-07	5.1e-05	6.0e-05	7.3e-06

Table 5-2 Non-exceedance probabilities for 7 m offset limit (Deepsea Bergen)

<i>H_s \ T_p</i>	4 s	5 s	6 s	7 s	8 s	10 s	12 s	14 s	16 s
3 m	0.9735	0.4009	0.5075	0.99928	0.99994	1	1	1	1
4 m	-	0.0008	0.0024	0.86196	0.98431	0.9967	0.99993	0.99999	0.99992
5 m	-	-	2.3e-07	0.14625	0.6301	0.8183	0.98064	0.98928	0.98937
6 m	-	-	-	0.0012	0.0617	0.16804	0.6946	0.81939	0.82117
7 m	-	-	-	1.5e-06	0.0004	0.0024	0.12955	0.31542	0.2935

Table 5-3 Non-exceedance probabilities for 10 m offset limit (Deepsea Bergen)

<i>H_s \ T_p</i>	4 s	5 s	6 s	7 s	8 s	10 s	12 s	14 s	16 s
3 m	0.99942	0.89831	0.93153	1	1	1	1	1	1
4 m	-	0.09609	0.16449	0.99503	0.99983	0.99997	1	1	1
5 m	-	-	0.00065	0.7742	0.97257	0.98974	0.99986	0.99997	0.99998
6 m	-	-	-	0.16069	0.64595	0.78020	0.98667	0.99742	0.99839
7 m	-	-	-	0.00495	0.12121	0.22498	0.82571	0.96365	0.97029

Table 5-4 Non-exceedance probabilities for 14 m offset limit (Deepsea Bergen)

<i>H_s \ T_p</i>	4 s	5 s	6 s	7 s	8 s	10 s	12 s	14 s	16 s
3 m	1	0.99446	0.99682	1	1	1	1	1	1
4 m	-	0.60911	0.71089	0.99996	1	1	1	1	1
5 m	-	-	0.07246	0.98567	0.99947	0.9998	1	1	1
6 m	-	-	-	0.73982	0.96883	0.98236	0.99984	0.99999	1
7 m	-	-	-	0.23681	0.71881	0.80054	0.99192	0.99973	0.99986

Table 5-5 Non-exceedance probabilities for 20 m offset limit (Deepsea Bergen)

<i>H_s \ T_p</i>	4 s	5 s	6 s	7 s	8 s	10 s	12 s	14 s	16 s
3 m	1	0.99994	0.99997	1	1	1	1	1	1
4 m	-	0.95653	0.97463	1	1	1	1	1	1
5 m	-	-	0.59024	0.99985	1	1	1	1	1
6 m	-	-	-	0.98224	0.99951	0.99966	1	1	1
7 m	-	-	-	0.83113	0.98296	0.98801	0.99993	1	1

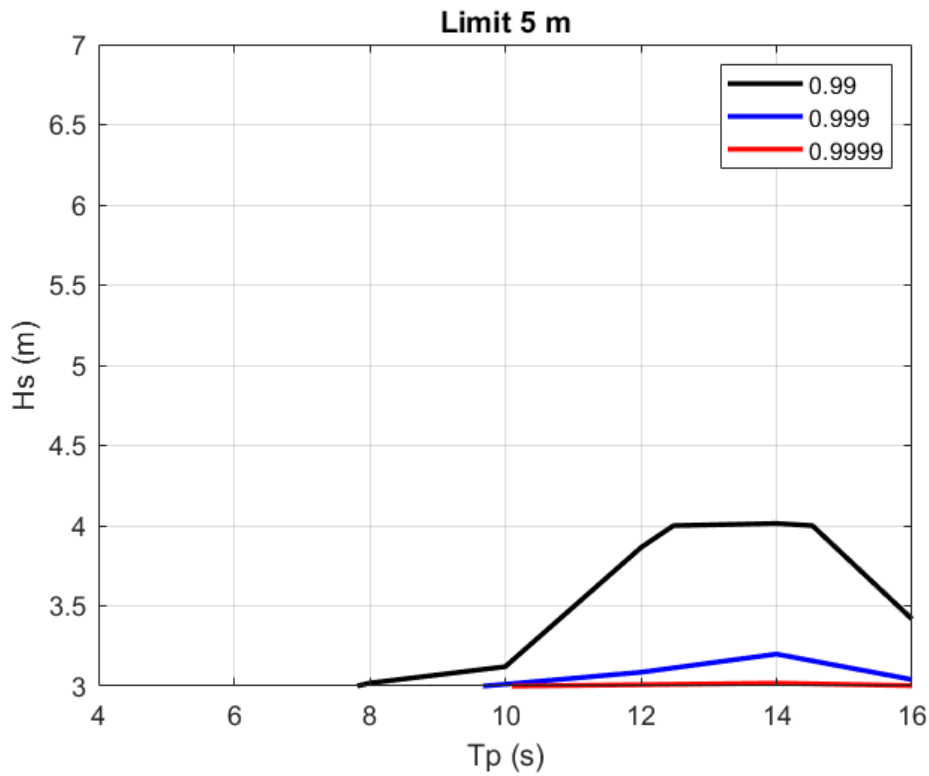


Figure 5-1 *Hs-Tp* contour lines of non-exceedance probability for offset limit 5 m and probability levels 0.99, 0.999 and 0.9999 (Deepsea Bergen)

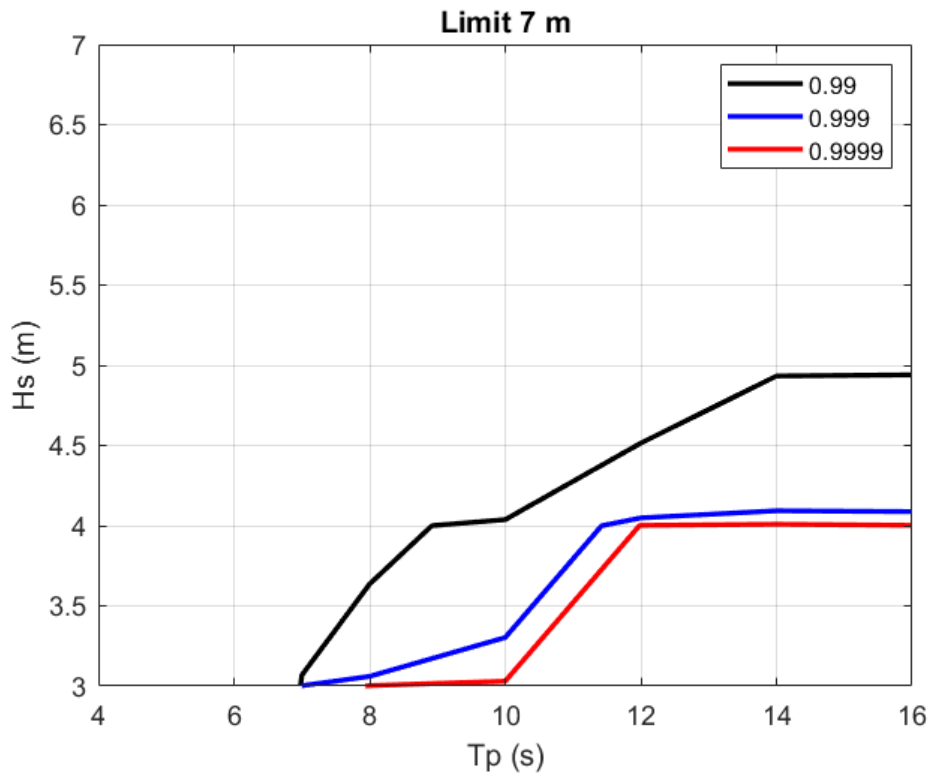


Figure 5-2 *Hs-Tp* contour lines of non-exceedance probability for offset limit 7 m and probability levels 0.99, 0.999 and 0.9999 (Deepsea Bergen)

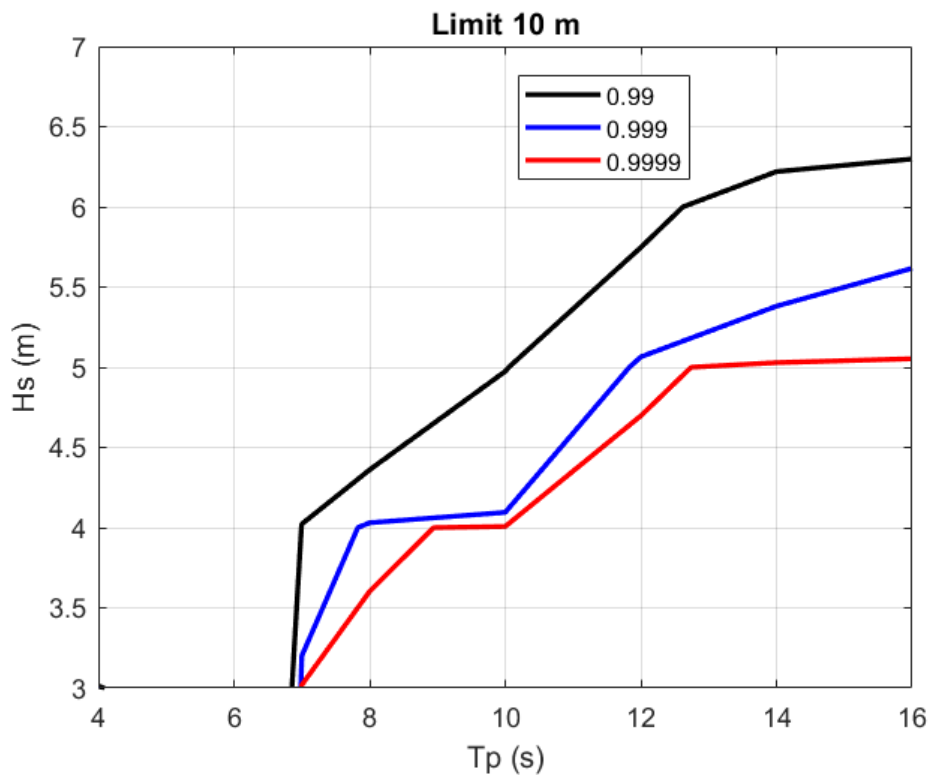


Figure 5-3 *Hs-Tp* contour lines of non-exceedance probability for offset limit 10 m and probability levels 0.99, 0.999 and 0.9999 (Deepsea Bergen)

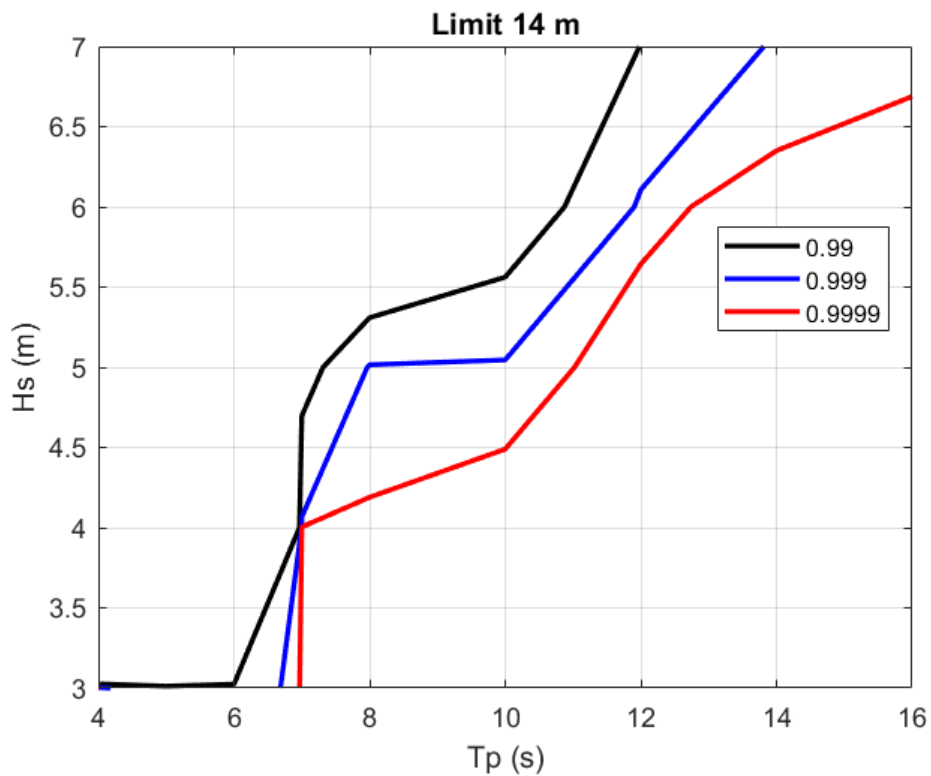


Figure 5-4 *Hs-Tp* contour lines of non-exceedance probability for offset limit 14 m and probability levels 0.99, 0.999 and 0.9999 (Deepsea Bergen)

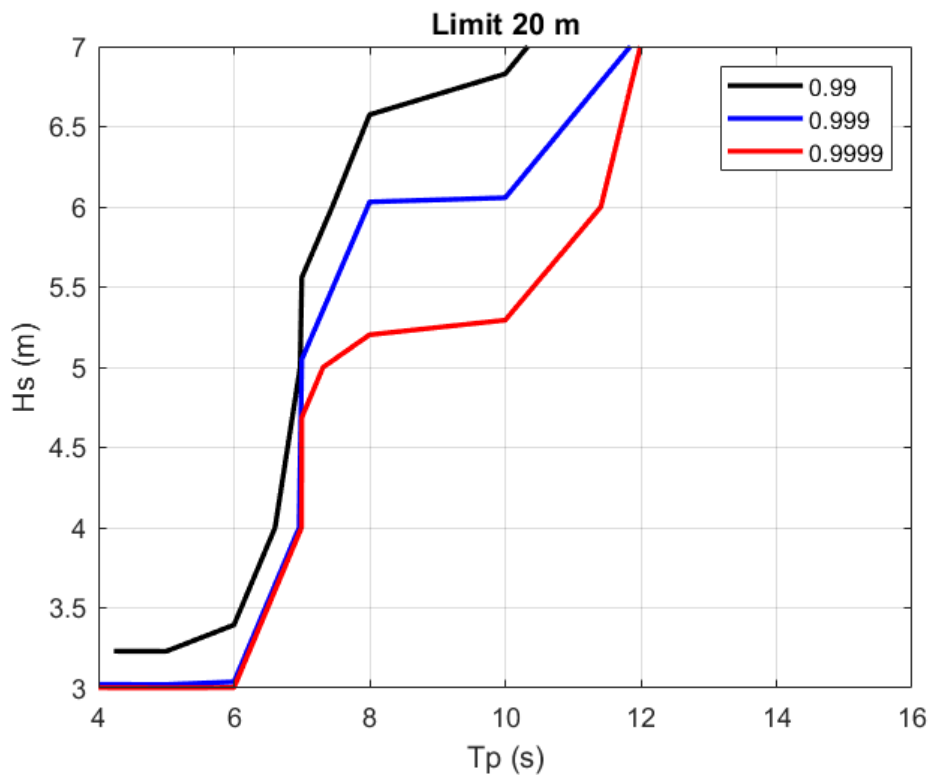


Figure 5-5 *Hs*-*Tp* contour lines of non-exceedance probability for offset limit 20 m and probability levels 0.99, 0.999 and 0.999 (Deepsea Bergen)

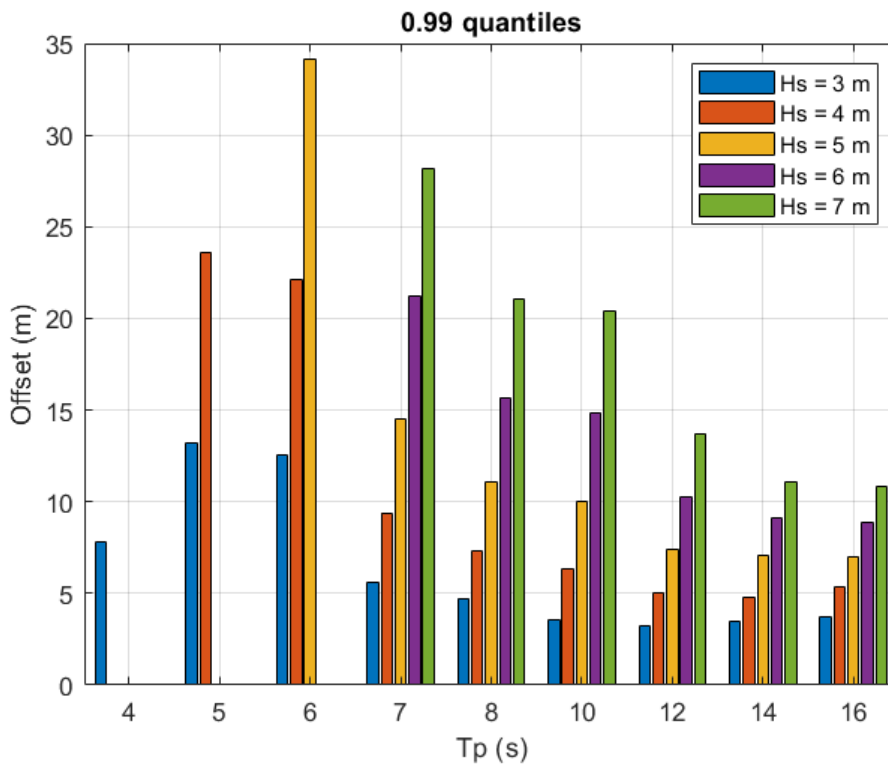


Figure 5-6 0.99 quantiles of surge offset (Deepsea Bergen)

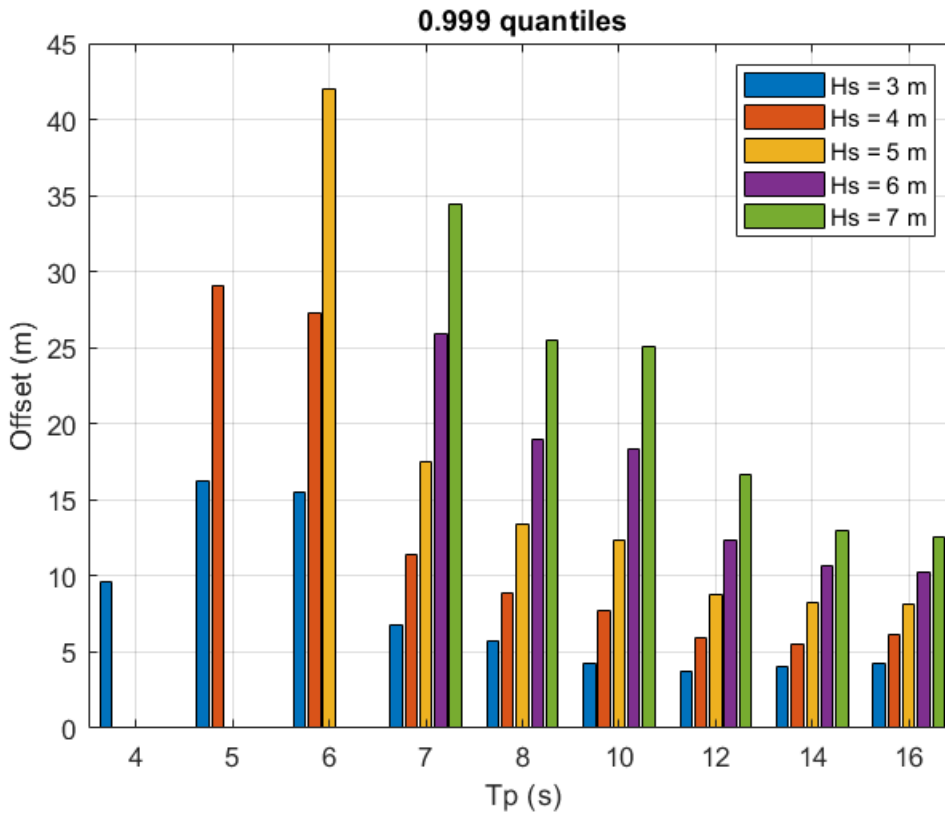


Figure 5-7 0.999 quantiles of surge offset (Deepsea Bergen)

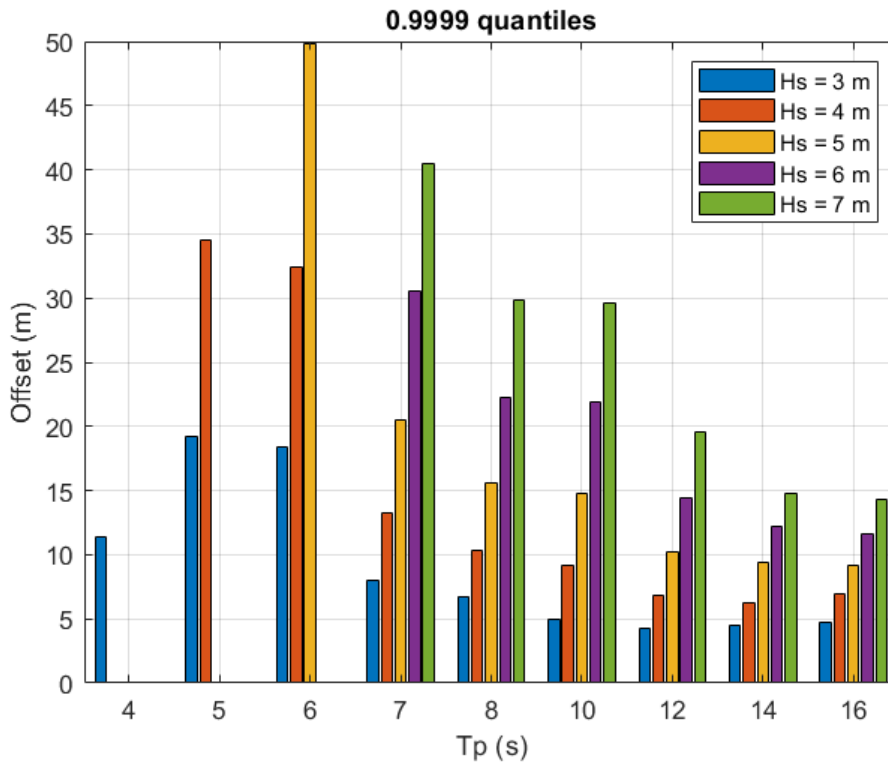


Figure 5-8 0.9999 quantiles of surge offset (Deepsea Bergen)

5.3 Results for the Exwave semi

The same calculations as in the previous section were carried out for the Exwave semi. The results are presented in Table 5-1 - Table 5-5 and Figure 5-9 - Figure 5-16. Comparing with the results for Deepsea Bergen in subsection 5.2, the probabilities of limit exceedance are more or less the same.

Table 5-6 Non-exceedance probabilities for 5 m offset limit (Exwave semi)

$H_s \setminus T_p$	4 s	5 s	6 s	7 s	8 s	10 s	12 s	14 s	16 s
3 m	0.95179	0.94996	0.52919	0.98529	0.99943	0.9997	1	1	1
4 m	-	0.15253	0.00285 43	0.41822	0.84784	0.91122	0.98739	0.99972	0.99994
5 m	-	-	1.7e-07	0.00657	0.08487	0.11775	0.59966	0.93403	0.98443
6 m	-	-	-	2.2e-06	0.00016	6.1e-05	0.04845	0.36506	0.68487
7 m	-	-	-	1.7e-10	2.7e-08	3.6e-09	0.00040	0.00889	0.08315

Table 5-7 Non-exceedance probabilities for 7 m offset limit (Exwave semi)

$H_s \setminus T_p$	4 s	5 s	6 s	7 s	8 s	10 s	12 s	14 s	16 s
3 m	0.99837	0.99844	0.92677	0.99947	1	1	1	1	1
4 m	-	0.73969	0.15666	0.88866	0.99097	0.99608	0.99983	1	1
5 m	-	-	0.00048	0.27295	0.66119	0.71625	0.96272	0.99916	0.99997
6 m	-	-	-	0.00569	0.08032	0.03662	0.60605	0.94689	0.99447
7 m	-	-	-	8.5e-06	0.00059	5.0e-05	0.14899	0.54289	0.89082

Table 5-8 Non-exceedance probabilities for 10 m offset limit (Exwave semi)

$H_s \setminus T_p$	4 s	5 s	6 s	7 s	8 s	10 s	12 s	14 s	16 s
3 m	0.99999	0.99999	0.99703	1	1	1	1	1	1
4 m	-	0.98276	0.72584	0.99392	0.99988	0.99997	1	1	1
5 m	-	-	0.07602	0.8483	0.9742	0.98109	0.99919	1	1
6 m	-	-	-	0.28874	0.71343	0.53665	0.96536	0.99938	0.99999
7 m	-	-	-	0.01514	0.14777	0.03068	0.79162	0.97277	0.99917

Table 5-9 Non-exceedance probabilities for 14 m offset limit (Exwave semi)

$H_s \backslash T_p$	4 s	5 s	6 s	7 s	8 s	10 s	12 s	14 s	16 s
3 m	1	1	0.99996	1	1	1	1	1	1
4 m	-	0.99966	0.97068	0.99988	1	1	1	1	1
5 m	-	-	0.5525	0.99004	0.99941	0.99962	0.99999	1	1
6 m	-	-	-	0.83781	0.98099	0.93932	0.99892	1	1
7 m	-	-	-	0.36026	0.75200	0.43572	0.98548	0.99957	1

Table 5-10 Non-exceedance probabilities for 20 m offset limit (Exwave semi)

$H_s \backslash T_p$	4 s	5 s	6 s	7 s	8 s	10 s	12 s	14 s	16 s
3 m	1	1	1	1	1	1	1	1	1
4 m	-	1	0.9992	1	1	1	1	1	1
5 m	-	-	0.93824	0.99986	1	1	1	1	1
6 m	-	-	-	0.99115	0.9998	0.9982	0.99999	1	1
7 m	-	-	-	0.89125	0.98579	0.91258	0.99976	1	1

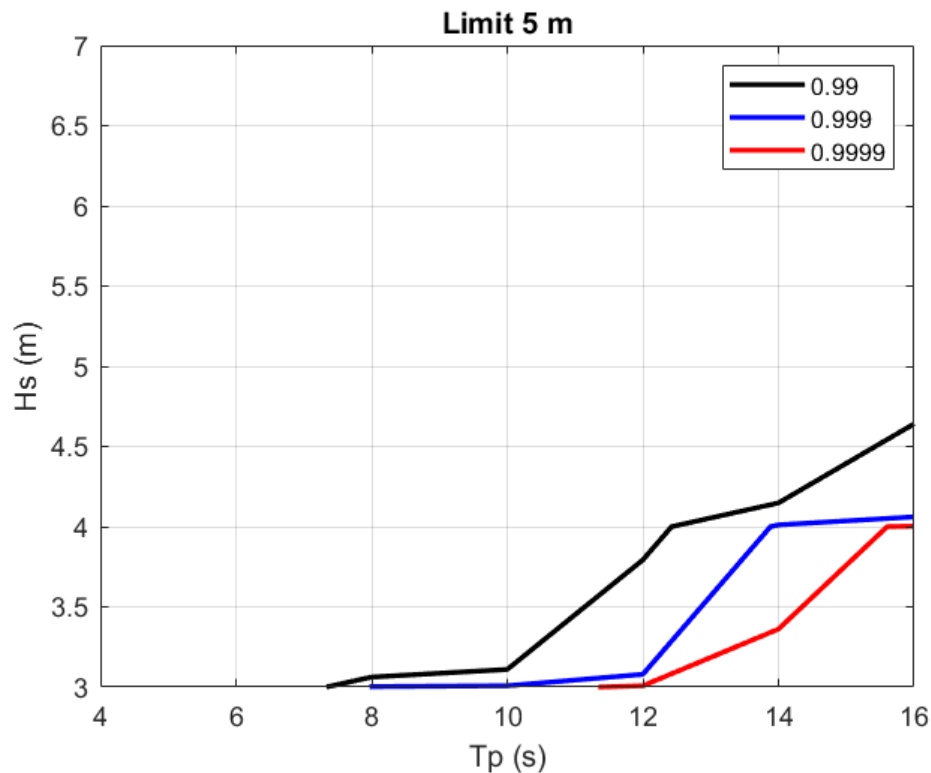


Figure 5-9 H_s - T_p contour lines of non-exceedance probability for offset limit 5 m and probability levels 0.99, 0.999 and 0.9999 (Exwave semi)

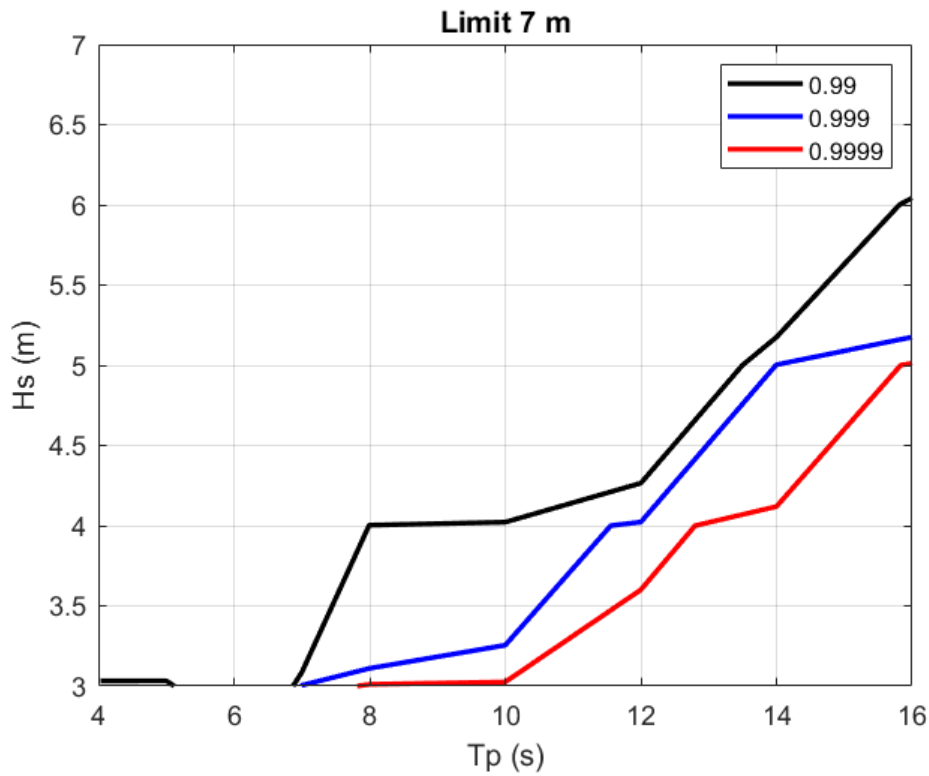


Figure 5-10 *Hs*-*Tp* contour lines of non-exceedance probability for offset limit 7 m and probability levels 0.99, 0.999 and 0.9999 (Exwave semi)

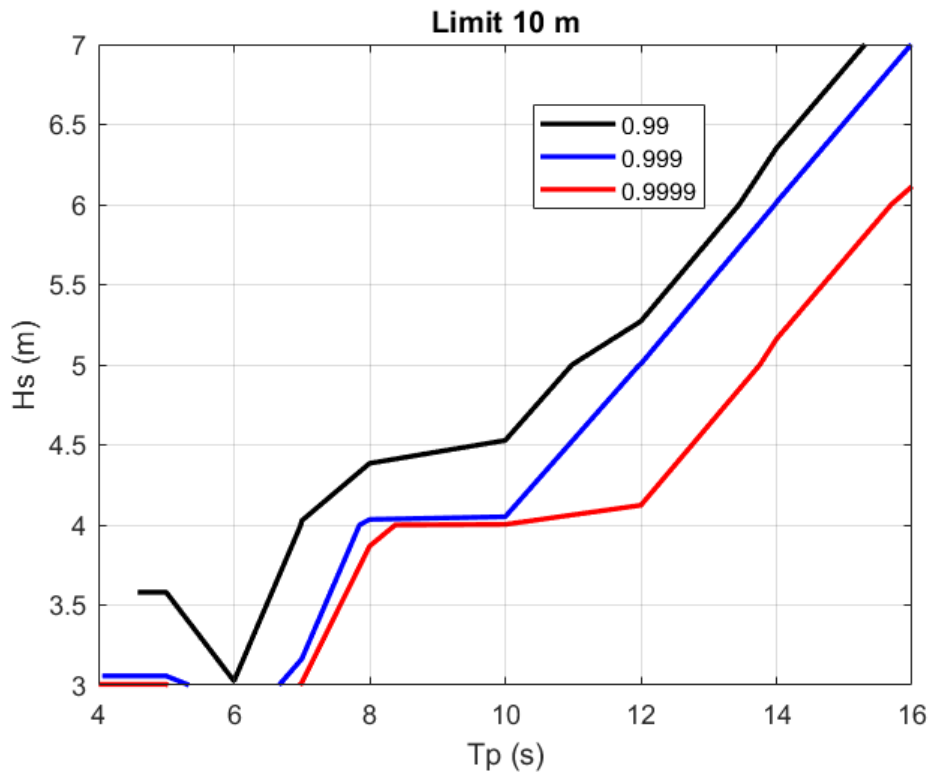


Figure 5-11 *Hs*-*Tp* contour lines of non-exceedance probability for offset limit 10 m and probability levels 0.99, 0.999 and 0.9999 (Exwave semi)

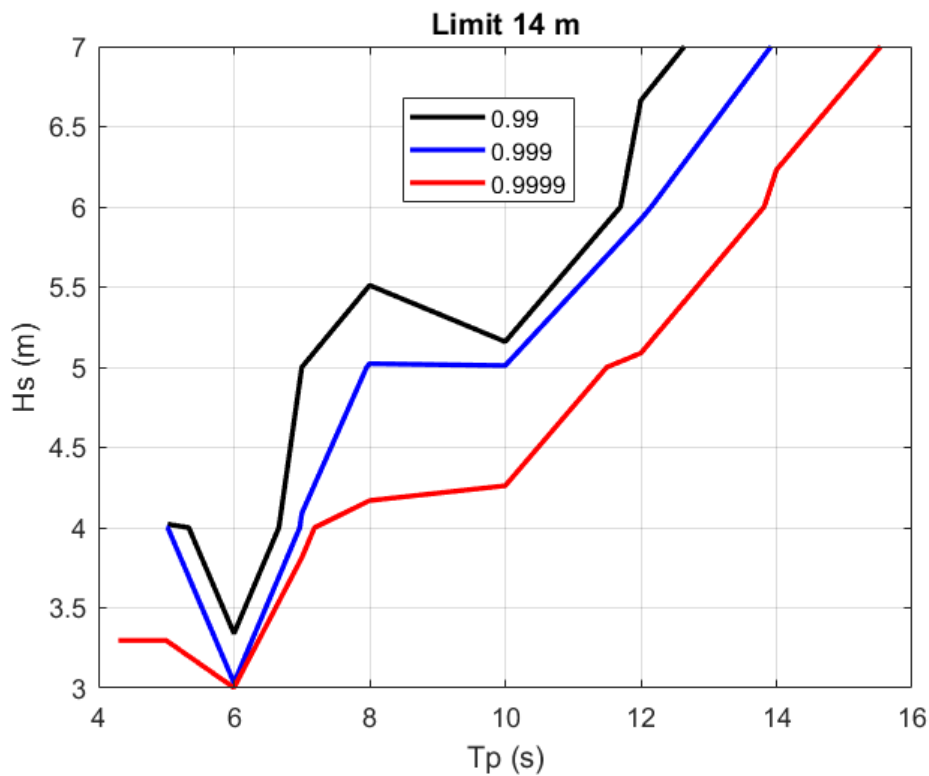


Figure 5-12 *Hs*-*Tp* contour lines of non-exceedance probability for offset limit 14 m and probability levels 0.99, 0.999 and 0.9999 (Exwave semi)

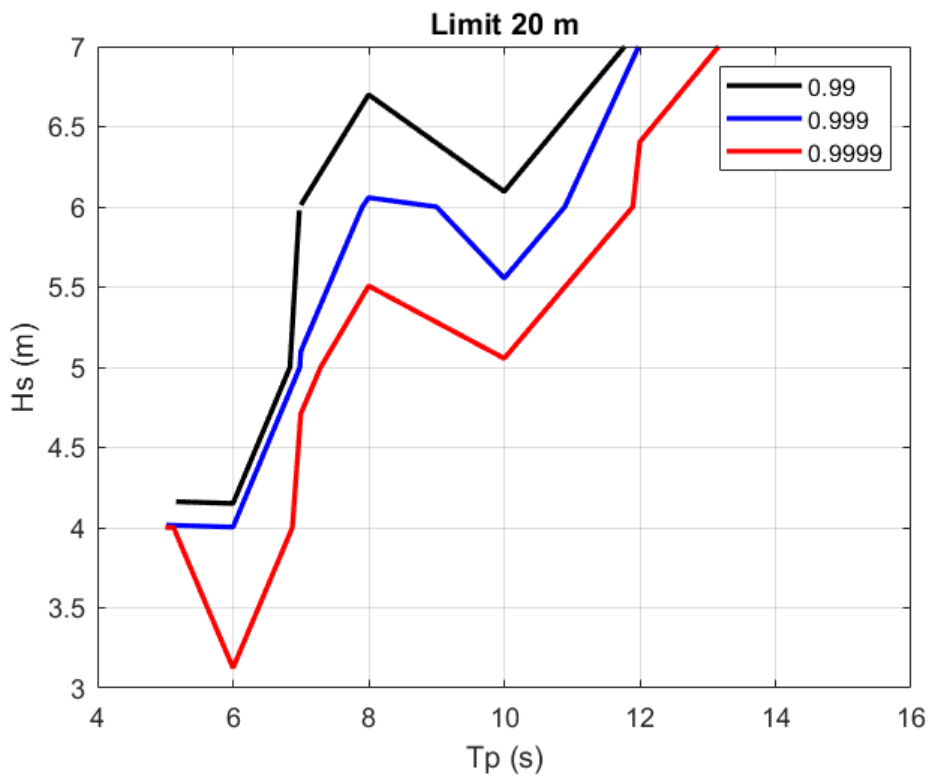


Figure 5-13 *Hs*-*Tp* contour lines of non-exceedance probability for offset limit 20 m and probability levels 0.99, 0.999 and 0.9999 (Exwave semi)

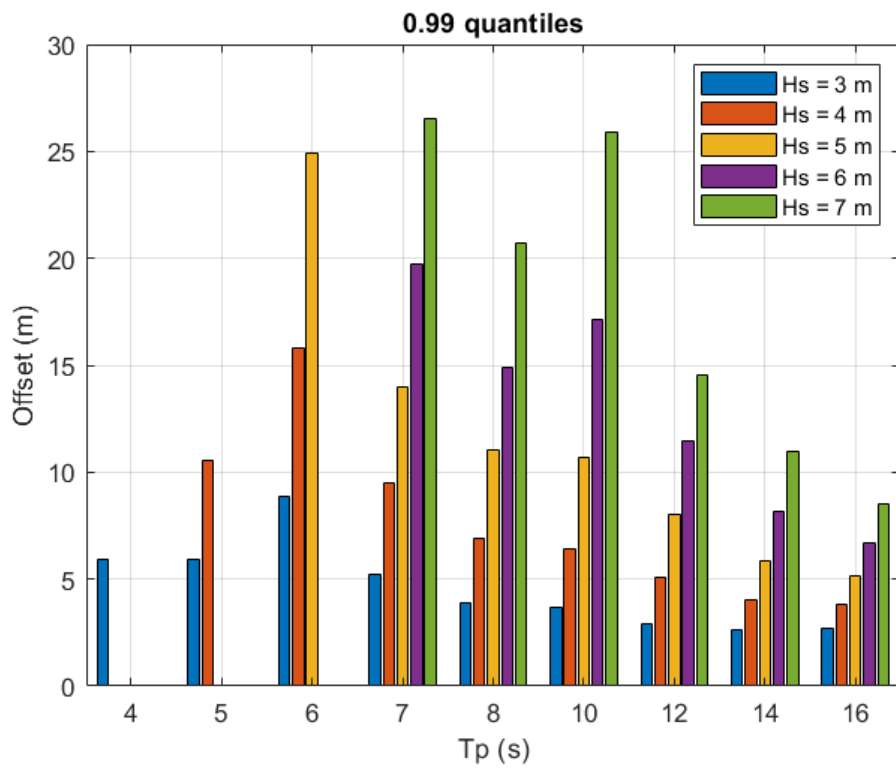


Figure 5-14 0.99 quantiles of surge offset (Exwave semi)

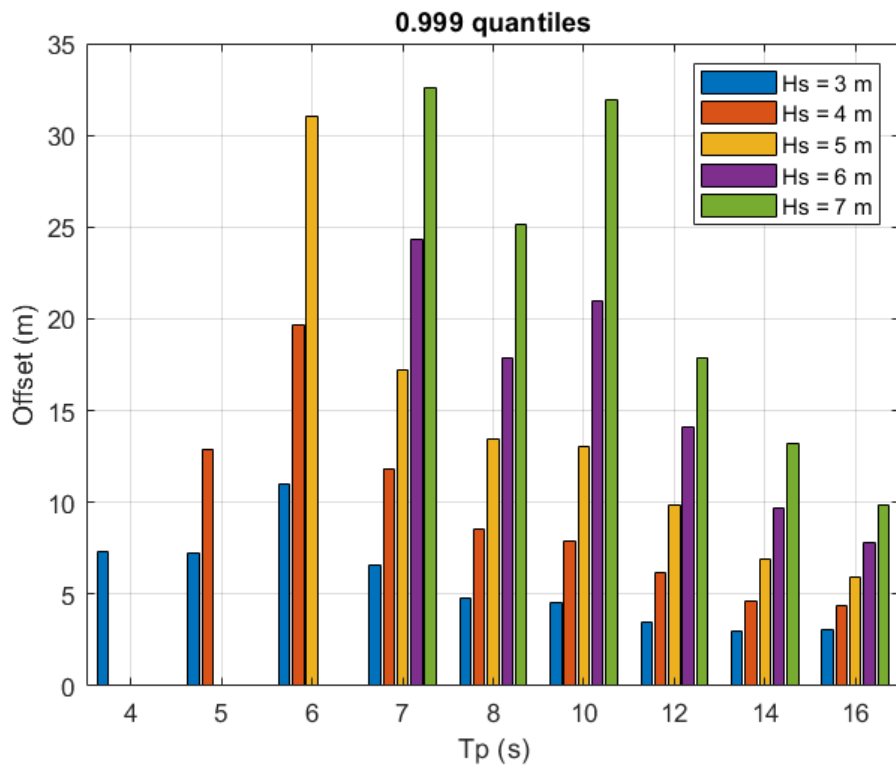


Figure 5-15 0.999 quantiles of surge offset (Exwave semi)

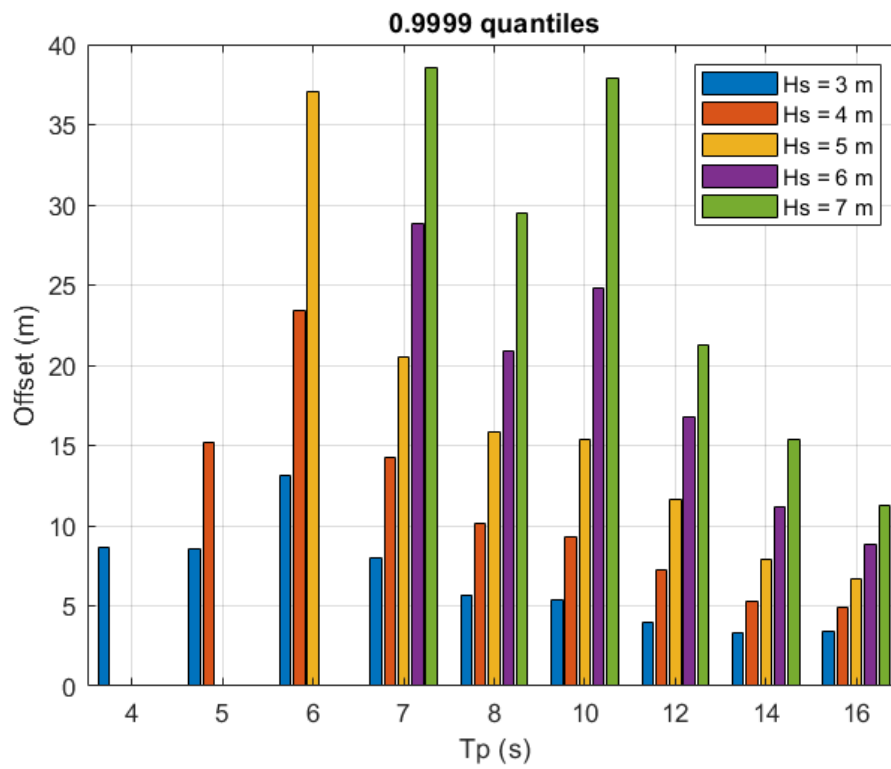


Figure 5-16 0.9999 quantiles of surge offset (Exwawe semi)

6 SUGGESTIONS FOR FURTHER WORK

From the study described above, further investigation could be devoted to the following topics:

6.1 Error analysis

For the data-driven approach, the error in the fitted Weibull parameters will be evaluated as a function of the data length. The effect of the uncertainty on the calculated probabilities of limit exceedance will be evaluated and used to correct the probabilities.

6.2 Choice of threshold

With the UPCROSSING method (Table 4-1) in combination with peaks-over-threshold, the value of the threshold will affect the estimated distribution parameters. A higher threshold will exclude lower peaks of response and may offer a better fit to the tail of the distribution, which is important for the extreme calculation. On the other hand, less data points will be available, which will increase the estimation error. Hence, there will be a trade-off between structural error and random error, with the threshold as the governing parameter for the optimal choice.

6.3 Theory-based approach and combining LF and WF extremes

The example in section 4.1 shows good agreement with the data-driven approach. A theoretical approach does not need very long simulated records of response, which requires efficient numerical tools. Therefore, a theory-based method, e.g. Stansberg's method [7], can be a favourable choice for the LF part of the response. A study of this should also include the possibility of finding a better way to combine LF and WF motion than the apparently crude method in Eq. (2).

6.4 Effect of rate limits

The DP system is usually designed to be predominantly linear, which means that the controller gains are constant factors, and the thrusters do not reach their limits within their designed range of operation. However, there may exist limits on the *rate of change*. The limit will exist on the rate of thruster force (kN/s) or on the turning speed for azimuth thrusters (degrees/s). In particular, the last type of limit can be a problem. To minimise its effect, sophisticated thruster allocation may be required. The effect of rate limits can be subtle and should be considered in an extreme value analysis.

6.5 Multi-mode and composite response criteria

In the present study, only surge motion has been considered, and the only limit has been on surge offset. In most operations, also other components of vessel motion will need consideration, and often the critical variable will be a combination of responses, like the motion of an eccentric point in the vessel (e.g. the end point of a gangway). In many cases, the critical variables will include velocities and accelerations in addition to or instead of the components of translational and angular position. For these variables, the WF part of response may be predominant. Hopefully, the methods considered herein will apply for such cases, but this should be checked.

7 CONCLUSION

The objective of the study has been to find a procedure for determining H_s - T_p criteria for interruption (or continuation) of on-going marine operations. The basic criteria for the operation are given as limits on the vessel response, but it is assumed that any such limit can be expressed as a set of H_s - T_p pairs. The scope of the study is limited to considering the wave-induced surge offset. Both LF and WF motions are considered.

The data material for the study has been response simulated with SIMO using numerical models for two semi-submersible vessels (Deepsea Bergen and the Exwave semi) with thrusters and DP controller. To study the dynamic response process and develop methods for estimation of extreme response, a *base case* constituted by the Deepsea Bergen model and a wave state of $H_s = 5$ m, and $T_p = 11.8$ s was chosen. This wave state gives LF and WF surge responses that both are significant. For the base case, a simulated record of 100 hours duration was simulated with SIMO.

The method of extreme value estimation used in the study, includes two steps. First a parametric distribution function is fitted to the response's upward peaks. Then, using the average time distance between the peaks, the CDF for the extreme value in a given interval of time (e.g. 3 hours) can be found. From the CDF, any quantile of surge response can be determined.

The LF and WF parts of the response are distributed very differently. The WF peaks are known to be distributed according to the Rayleigh distribution, provided the spectral bandwidth is small. For the base case environment this was confirmed. The LF response is much more complicated, but its distribution of peaks is expected to be close to the exponential distribution. According to theory, this is expected for a dynamically positioned vessel, which is strongly damped.

To circumvent the problem of combining the extremes of LF and WF response into a common, total extreme response, it was attempted to fit a distribution to the total (LF+WF) response. It turned out that this could be done with the three-parameter Weibull distribution, taking the maxima between instants of up-crossing and down-crossing and choosing a suitable threshold for the peaks. In addition to the base case environment, this distribution was tested on two wave states of respectively less and more WF content than the base case. The Weibull distribution proved to give good results for these wave states too.

The approach of estimating a distribution to simulated data requires long simulation time, due to the slowness of the LF process and its exponential nature, which causes the extremes to occur rarely and with large spread. A fast and powerful simulation tool, like SIMO may be required. A theory-based approach is an alternative. It requires only second-order statistics and requires shorter simulation time. With this approach, the LF and WF statistics are treated separately and must be combined into a common result for the total (WF+LF) response. How to do the combination is not trivial. An established rule-of-thumb simplified method, exists, however. The theoretical approach was tested on the base case and found to give very good agreement with the data.-driven approach. However, to draw a general conclusion on the applicability of the theoretical approach, more cases must be studied.

For estimation of extreme response using a distribution derived from data, it is important that the dynamic process of vessel response is *smooth* in the domain of intended operation. This implies that there must be no discontinuities in the response variables and their time-derivatives up to some sufficient order. While the wave-loading process is continuous, the response may not be so if there are limits in the thruster system or breaks in the positioning characteristic.

To interrupt a marine operation and secure equipment and personnel due to forthcoming adverse weather will take a certain time. If, during this time, the required probability of not exceeding a response limit is given, the corresponding H_s - T_p limit will depend on the duration of the interrupt operation (the longer the duration, the milder the limiting wave state must be). Hence the H_s - T_p criteria will depend on duration. An example of this is given in the study.

To account for uncertainty in the weather forecast, it is customary to reduce the permissible H_s by a so-called alpha factor. In calculations of probability of limit exceedance, it is suggested to use wave heights modified by the *inverse* alpha factor. An example of the effect of this modification is given.

For 36 combinations of H_s and T_p , five offset limits and three values of non-exceedance, probability quantiles of response and probabilities of limit exceedance are calculated for the two semi-submersibles. The results are presented in the form of tables, bar plots and contour plots.

The study has been limited to consider wave-induced surge offset and limits for this variable. Suggestions for further topics of study are given, including error analysis, more complex responses and criteria, use of theoretical approach and combination of LF and WF statistics and rate limits in thruster system.

8 ACKNOWLEDGEMENT

SINTEF Ocean thanks Odfjell Drilling AS for permission to use the numerical model for Deepsea Bergen in the study.

9 REFERENCES

- [1] Leira, B., Moan, T., Haver, S., Spidsøe N., "TMR4235 Stochastic Theory of Sealoading, Probabilistic Modelling and Estimation", Lecture notes, Department of Marine Technology, Faculty of Engineering Science and Technology – NTNU Trondheim Norwegian University of Science and Technology, 2005
- [2] Myrhaug, D., "Uregelmessig sjø", Kompendium SIN1015 Marin dynamikk, Faculty of engineering Science and Technology – NTNU Trondheim Norwegian University of Science and Technology, 2002
- [3] Fonseca, N., Ommani, B., Stansberg, C. T., Bøckmann, A., Birknes-Berg, J., Nestegård, A., de Haute-cloque, G., Baarholm, R., "Wave Forces and Low Frequency Drift Motions in Extreme Seas: Benchmark Studies", Paper OTC-27803-MS, Offshore Technology Conference, Houston, USA, 2017
- [4] DNV GL, "Position mooring", Offshore standards, DNVGL-OS-E301, July 2018
- [5] SIMO 4.18.2 User Guide SINTEF Ocean, December 10, 2020
- [6] MIMOSA User's Documentation, Program version 6.3-10, SINTEF Ocean, 2019-10-01
- [7] Stansberg, C. T., "Prediction of Extreme Slow-Drift Amplitudes", Paper No. 00-6135 Proc. 19th OMAE Conference (ASME), New Orleans, LA, USA, 2000
- [8] SINTEF Ocean, "Possibility of loss of position for dynamically positioned semi-submersibles due to impulsive wave load", Report No. OC2021 F-079, SINTEF Ocean, Trondheim, Norway, 2021-09-30
- [9] DNVGL-ST-N101 Marine Operations, DNV 2016, Ed. 2016-06
- [10] DNV-OS-H101 Offshore Standard, "Marine Operations, General", October 2011
- [11] DNV-OS-H102 Offshore Standard, "Marine Operations, Design and Fabrication, January 2012
- [12] DNV-ST-0358_Certification of offshore GW for personnel transfer, ver 2021
- [13] DNV-W2W-Industry Guidance_ver. 2015
- [14] Online calculator: The waves and the wind. Wave height statistical forecasting. <https://planetcalc.com/4442/>

- [15] ISO 19901-1 Petroleum and natural gas industries — Specific requirements for offshore structures — Part 1: Metocean design and operating considerations
- [16] Næss, A., "Prediction of extremes of combined first-order and slow-drift motions of offshore structures", Applied Ocean Research, 1989, Vol 11, No. 2
- [17] Næss, A., "Effects of correlation on extreme slow-drift response", Eighth International Conference on Offshore Mechanics and Arctic Engineering, The Hague, March 19-23, 1989.